Removing polymeric coatings with nanostructured fluids: influence of substrate, nature of the film, and application methodology

Michele Baglioni[1], Margherita Alterini[1], David Chelazzi[1], Rodorico Giorgi[1*], Piero Baglioni[1*]

[1]University of Florence, Italy

Conflict of interest statement

The authors declare that the research was conducted in the absence of any commercial or financial relationships that could be construed as a potential conflict of interest

Author contribution statement

M.B, M.A., and D.C. contributed to the conception and design of the work, to the acquisition, the analysis, and the interpretation of experimental data.
R.G. and P.B. revised the work critically giving a substantial intellectual contribution, and ultimately provided the final approval for its publication.

Keywords

Abstract

 Word count: 291

Cleaning is one of the most important and delicate operations in the conservation of cultural heritage, and, if not correctly performed, may irreversibly damage works of art. The removal of aged or detrimental polymeric coatings from works of art is a common operation in conservation, and nanostructured fluids (NSFs), such as aqueous swollen micelles and oil-in-water (o/w) microemulsions, are used as an alternative to non-confined organic solvents that pose a series of non-negligible drawbacks. NSFs effectiveness in removing polymeric coatings has been thoroughly demonstrated in the last decades, while their cleaning mechanism is still under investigation. The present work deepens the knowledge on the removal mechanisms of NSFs, studying the interaction of a four-component NSF with four different types of acrylic and vinyl polymer films cast from solutions or aqueous polymer latexes on three substrates (glass, marble and polystyrene) with different hydrophilicity and wettability. NSFs were applied either as non-confined or confined in cellulose poultices (traditionally employed by conservators), or in highly retentive chemical gels, observing the influence of the confining matrix on the removal process. It was found that the NSF/polymer film interaction is greatly dependent on the film structure and composition. Films formed from solvent solutions can be swollen by water/organic solvents mixtures or dewetted when a surfactant is added to the cleaning fluid; films formed from polymer latexes, on the other hand, are generally swollen even just by water alone, but poorly dewet. The substrate also plays an important role in the removal of polymer films formed from solutions, for instance the removal of an acrylic polymer from polystyrene could be achieved only through highly selective cleaning using NSF-loaded chemical hydrogels. These results can be key for conservators, providing innovative solutions to face new challenges in art preservation.

Contribution to the field

The development of innovative materials for conservation of cultural heritage poses a twofold challenge; on one side they need to meet the expectations and need of conservators and restorers from a purely applicative standpoint, while, on the other, their phyisico-chemical interaction with artworks' materials need to be thoroughly understood. This paper provides not previously reported results on the removal of polymeric coatings by means of nanostructured fluids. The different behavior of polymer films cast from solvents' solutions with respect to films formed from aqueous polymer latexes is explored and described for the very first time, here, improving the knowledge about physico-chemical properties of such materials. Finally, the influence of the substrate on polymer films removal is systematically studied for the first time, and it was shown that, when the affinity between the polymer coating and the substrate it is laid on is particularly high, the optimal way to selectively and completely remove it is to confine a nanostructured fluid into a highly-retentive hydrogel, which enhance the control on the cleaning action. We believe that both conservators and scientists can find their interest in reading this paper.

Funding statement

Ethics statements

Studies involving animal subjects
Generated Statement: No animal studies are presented in this manuscript.

Studies involving human subjects
Generated Statement: No human studies are presented in this manuscript.

Inclusion of identifiable human data
Generated Statement: No potentially identifiable human images or data is presented in this study.

Data availability statement

Generated Statement: The datasets generated for this study will not be made publicly available The relevant data are already completely and clearly reported in the paper..

Removing polymeric coatings with nanostructured fluids: influence of substrate, nature of the film, and application methodology

1 **Michele Baglioni[1o], Margherita Alterini[1], David Chelazzi[1], Rodorico Giorgi[1]*, Piero Baglioni[1o]***

2 [1]Department of Chemistry and CSGI, University of Florence, via della Lastruccia, 3, 50019, Sesto
3 Fiorentino (FI), Italy.

4 ***Correspondence:**
5 Corresponding Authors
6 giorgi@csgi.unifi.it
7 baglioni@csgi.unifi.it

8

9 MAIN TEXT WORD COUNT: < 10 000

10 ABSTRACT WORD COUNT: 322

11

12 °No kinship exists among these authors.

13 **Keywords: polymer coatings, cleaning, nanostructured fluids, acrylics, vinyls, nonionic**
14 **surfactants, hydrogels, dewetting**

15 **Abstract**

16 Cleaning is one of the most important and delicate operations in the conservation of cultural heritage,
17 and, if not correctly performed, may irreversibly damage works of art. The removal of aged or
18 detrimental polymeric coatings from works of art is a common operation in conservation, and
19 nanostructured fluids (NSFs), such as aqueous swollen micelles and oil-in-water (o/w)
20 microemulsions, are used as an alternative to non-confined organic solvents that pose a series of non-
21 negligible drawbacks. NSFs effectiveness in removing polymeric coatings has been thoroughly
22 demonstrated in the last decades, while their cleaning mechanism is still under investigation. The
23 present work deepens the knowledge on the removal mechanisms of NSFs, studying the interaction
24 of a four-component NSF with four different types of acrylic and vinyl polymer films cast from
25 solutions or aqueous polymer latexes on three substrates (glass, marble and polystyrene) with
26 different hydrophilicity and wettability. NSFs were applied either as non-confined or confined in
27 cellulose poultices (traditionally employed by conservators), or in highly retentive chemical gels,
28 observing the influence of the confining matrix on the removal process. It was found that the
29 NSF/polymer film interaction is greatly dependent on the film structure and composition. Films
30 formed from solvent solutions can be swollen by water/organic solvents mixtures or dewetted when a
31 surfactant is added to the cleaning fluid; films formed from polymer latexes, on the other hand, are
32 generally swollen even just by water alone, but poorly dewet. The substrate also plays an important
33 role in the removal of polymer films formed from solutions, for instance the removal of an acrylic
34 polymer from polystyrene could be achieved only through highly selective cleaning using NSF-

35 loaded chemical hydrogels. These results can be key for conservators, providing innovative solutions
36 to face new challenges in art preservation.

37

38 **1. Introduction**

39 Cleaning of works of art generally consists in the selective removal of materials that promote the
40 degradation of the artifacts or alter their readability and appearance. Among these materials, aged or
41 detrimental polymeric coatings are often found on works of art, and their removal is a common
42 operation in art conservation. Synthetic polymers have been largely employed in the traditional
43 restoration practice as varnishes, adhesives, protectives and consolidating agents. The presence of
44 polymeric coatings on the surface of porous inorganic substrates (wall paintings, stone, mortars)
45 drastically reduces water permeability and enhances the degradation induced by salts, up to
46 consistent loss of the artifacts' surface layers (Carretti and Dei, 2004; Giorgi et al., 2010). Graffiti
47 and vandalism are other well-known examples where selective removal of polymeric coatings must
48 be carried out on artistic surfaces (Apostol et al., 2011; Baglioni et al.; Giorgi et al., 2017; Sanmartín
49 et al., 2014). Other cases include the removal of aged pressure sensitive tapes from paper artworks
50 (Bonelli et al., 2018), or of discolored and cracked varnishes from paintings (Baglioni et al., 2018a;
51 Burnstock and Kieslich, 1996).

52 The vast amount of different solvent-sensitive materials found in classic and contemporary art poses
53 continuous challenges to the safe removal of detrimental coatings (Kavda et al., 2017). Traditionally,
54 restorers and conservators rely on the use of organic solvents to dissolve or swell unwanted materials.
55 Solvents are typically applied either as non-confined, using cotton swabs, or thickened in viscous
56 polymeric solutions and solvent gels (Baglioni et al., 2012c; Burnstock and Kieslich, 1996;
57 Burnstock and White, 2000). However, these methods exhibit poor control and scarce selectivity, or
58 involve the presence of residues from the cleaning system. In addition, health concerns arise from the
59 toxicity of most solvents used in restoration.

60 Alternatively, nanostructured fluids (NSFs) such as aqueous swollen micelles and oil-in-water (o/w)
61 microemulsions were proposed in the late 1980s for the removal of hydrophobic matter from porous
62 inorganic substrates (Borgioli et al., 1995). Their effectiveness in removing polymeric coatings from
63 different types of surfaces has been thoroughly demonstrated in the last decades (Baglioni et al.,
64 2010, 2012b, 2015a, 2015b, 2016, 2018c; Carretti et al., 2003, 2007). These NSFs are water-based
65 systems where limited amounts of solvents are found either in the dispersed (as nano-sized droplets
66 stabilized by surfactants) or in the continuous phase of the fluids. The large surface area developed
67 by the nano-sized droplets, and the synergistic action of solvents and surfactants, are responsible for
68 enhanced cleaning power, while the presence of the continuous aqueous phase limits the re-
69 deposition of detached hydrophobic matter on hydrophilic surfaces. Besides, being water-based,
70 aqueous NSFs have reduced toxicity as opposed to traditional solvents. A further improvement was
71 represented by the confinement of NSFs into retentive physical or chemical gels able to gradually
72 release the fluids at the gel-artifact interface, maximizing control over the cleaning action (Baglioni
73 et al., 2015c; Chelazzi et al., 2018).

74 While these systems represent the most advanced cleaning tools currently available to conservators,
75 the interaction mechanism of NSFs with polymeric coatings is still being investigated.

76 The removal of high molecular weight macromolecules does not follow the rules of classical
77 detergency. Studies performed on model samples, i.e. glass slides coated with an acrylate copolymer,

2

78   have shown that dewetting takes place when water-based NSFs are put in contact with the polymeric
79   coating (Baglioni et al., 2017, 2018b; Raudino et al., 2015, 201, 2017). The film swells and detaches
80   from the surface. This behavior was also observed on mortar samples coated with the same polymer
81   (Baglioni et al., 2018b). The nature of both the organic solvents and the surfactant(s) included in the
82   cleaning formulation was found to be of fundamental importance in the whole process. The solvents
83   swell the polymer and lower its glass transition temperature, increasing the mobility of the polymer
84   chains; the surfactant reduces the interfacial tension, kinetically promoting the detachment of the
85   polymer film from the surface, and initiating the dewetting process that eventually breaks down the
86   coating into separate polymer droplets.

87   Despite providing fundamental insights, previous studies on this subject depicted only a partial
88   picture of the interaction mechanisms between NSFs and polymeric coatings. Namely, all the studies
89   were conducted only on a single type of polymer, i.e. Paraloid B72® (poly(ethyl methacrylate/methyl
90   acrylate, 70:30) cast from solution. Only glass or mortars were considered as substrates. Besides,
91   simplified NSFs formulations were used to isolate the contribution of individual components in the
92   system.

93   The present work aims to deepen the knowledge on the removal mechanisms of NSFs, studying the
94   interaction of a four-component NSF with four different types of polymer films cast either from
95   solutions or aqueous emulsions. In fact, it is well known that films of polymers cast from solutions
96   have different physical structures than those cast from emulsions (Chevalier et al., 1992; Steward et
97   al., 2000; Winnik, 1997), and polymers emulsions contain several additives; these can be crucial
98   factors in determining the interaction process with the NSFs. Three substrates were considered (glass,
99   marble and polystyrene) with different hydrophilicity and wettability. Finally, NSFs were applied
100   either as non-confined or confined in cellulose poultices (traditionally employed by conservators), or
101   in highly retentive chemical gels, observing the influence of the confining matrix on the removal
102   process.

103   The NSF is composed of water, an alcohol ethoxylate nonionic surfactant, 2-butanol (BuOH), and 2-
104   butanone (methyl ethyl ketone, MEK), and is representative of formulations actually employed in the
105   conservation practice for the cleaning of real works of art.

106   The three selected substrates were coated with the four different polymers, obtaining a set of 12
107   samples, which were then exposed to the NSF, investigating the interaction mechanism for each
108   combination. The effects of the NSF on the films were studied by means of optical microscopy and
109   micro-reflectance infrared Fourier Transform spectroscopy 2D mapping of the areas of interest,
110   which provides spatial resolution down to the micron-scale.

111   **2. Materials and methods**

112   **2.1. Chemicals**

113    $C_{9-11}E_{5,5}$ alcohol ethoxylate (Berol 266, AkzoNobel), sodium dodecylsulfate (SDS, Sigma-Aldrich,
114   purity $\geq$ 99%), butanone (MEK, Sigma-Aldrich, purity 99%), 2-butanol (BuOH, Sigma-Aldrich,
115   pority 99%), ethanol (EtOH, Fisher Chemical, purity $\geq$ 99%), white spirit (White Spirit, Fidea), D_2O
116   (EurisoTop, 98%), and deuterated butanone (d-MEK, $C_4H_3D_5O$, Sigma-Aldrich, purity 98%) were
117   used as received, without further purification. Water was purified with a Millipore Milli-Q gradient
118   system (resistance > 18 MΩ cm).

119

120

2.2. Polymers formulations

122 The four polymeric materials selected are widely used in the traditional restoration practice. They
123 include: poly(vinyl acetate) (PVAc), commercially known as PVA K40®, dissolved in ethanol;
124 PVAc as an aqueous emulsion, commercially known as Vinavil NPC®; poly(butyl methacrylate)
125 (PBMA) dissolved in white spirit, commercially known as Plexisol P550®; poly(ethyl
126 acrylate/methyl methacrylate) (PEA/PMMA) 40:60 as an aqueous emulsion, commercially known as
127 Plextol B500®. **Table 1** reports the main properties of the formulations. All the products were
128 applied on the substrates as a 10% (w/w) solution/emulsion.

129 **Table 1.** Main properties and sample names of the four commercial polymers used.

Commercial name	Polymer nature	Physical appearance	Dry matter content	Applied as	Sample name[a]	Film density (g/cm^3)[b]	Tg (°C)[c]
PVA K40®	PVAc	Transparent grains	-	10% solution in EtOH	V$_S$	1.27	31
Vinavil NPC®	PVAc	Aqueous emulsion	52%	10% aqueous emulsion	V$_E$	1.05	16
Plexisol P550®	PBMA	40% solution in white spirit	40%	10% solution in white spirit	A$_S$	1.08	28
Plextol B500®	PEA/PMMA	Aqueous emulsion	50%	10% aqueous emulsion	A$_E$	1.03	30

130 [a]V = vinyl; A = acrylic; S = polymer applied as a solution; E = polymer applied as an emulsion. [b]The density was
131 calculated as described in Section 2.3. [c]The glass temperature (Tg) was measured by means of DSC analyses according to
132 the procedure described in Section 2.2.1.

133

134 2.2.1. Differential scanning calorimetry (DSC) for the glass temperature (Tg) determination

135 DSC measurements were performed on a DSC Q1000 from TA Instruments on small samples (2-5
136 mg) of the four dry films, according to the following procedure: equilibration at -50 °C; heating ramp
137 from -50°C to 60°C at 10 °C/min; cooling ramp from 60 °C to -50 °C 10°C/min; heating ramp from -
138 50°C to 60°C at 10 °C/min. The first heating/cooling ramp was used to equilibrate the sample, while

139 the second heating ramp is the one used for the Tg determination. Each sample was run at least twice,
140 in order to check for reproducibility of the measurement.

141

2.3. Substrates

143 The three different substrates selected for this work, i.e., glass, marble and polystyrene, were selected
144 as they exhibit different wettability and are representative of artistic substrates frequently found in
145 classic or contemporary art production. Glass slides of $5 \times 5 \times 0.3$ cm^3, marble tiles of $5 \times 5 \times 1$ cm^3,
146 and polystyrene slides of $5 \times 5 \times 0.2$ cm^3 were used. The four different filming materials (polymers
147 solutions or emulsions) were then laid manually on the top surfaces of each series of samples. 150 µl
148 of each polymer formulation (V_S, V_E, A_S, A_E) was carefully and homogeneously spread on a 4×5
149 cm^2 area on the surface of glass, marble and polystyrene samples. A reference area was thus left
150 untreated. The specimens were left drying for 30 days, and then the dry mass of the films was
151 evaluated. The density of the dry films was then measured, by drying for 4 days in a ventilated oven
152 at 60 °C weighed amounts of polymer solutions/emulsions that were poured into graduated vials. The
153 results, reported in **Table 1**, made possible to calculate that the obtained films had an average
154 thickness of approximately 5-7 µm, assuming that they are homogeneously spread all over the treated
155 surface.

156

2.4. Attenuated total reflectance Fourier-transform infrared spectroscopy

158 ATR measurements were carried out with a Thermo Nicolet Nexus 870 spectrometer equipped with a
159 liquid nitrogen-cooled MCT detector and a single reflection diamond crystal ATR unit. Spectra were
160 recorded in the 4000-650 cm^{-1} range (128 scans, 4 cm^{-1} resolution). ATR measurements were
161 performed on small samples of spray-can paints' dried films, removed from the glass support.

162

2.5. NSF preparation

164 The NSF selected for this work is composed as follows (w/w): H_2O, 65.9%; $C_{9-11}E_{5,5}$, 3.5%; BuOH,
165 9.7%; MEK, 20.9%. In order to better understand the role of each component in the interaction with
166 the polymer coatings, other liquid systems were also used, obtained removing some of the
167 components from the complete NSF formulation. Namely, a water/$C_{9-11}E_{5,5}$ surfactant solution, and a
168 water/BuOH/MEK solvents mixture were used. In both systems, the ratio between each component
169 was the same as in the complete NSF formulation. It is worth noting that both BuOH and MEK are
170 partly water-miscible (12.5% and 24% at 20°C, respectively (Verschueren, 2001)) and this made
171 possible to obtain a single-phase stable mixture of water and solvents even in the absence of
172 surfactants.

173

2.6. Small-Angle Neutron Scattering

175 Small-angle neutron scattering (SANS) experiments were performed on the spectrometer V4 (Bensc-
176 Helmholtz Zentrum Berlin). Two different configurations were employed (i.e., sample-to-detector

177 distances, SD = 2 or 8 m) to cover a range of wave vectors q ($q = (4\pi/\lambda)\sin(\theta/2)$, where λ is the
178 wavelength of the incident neutron beam and θ the scattering angle) from 0.007 to 0.28 Å^{-1}. For each
179 configuration a 6 Å neutron wavelength was used and the wavelength resolution, $\Delta\lambda/\lambda$, was less than
180 10%. Samples were contained in 1 mm thick quartz cells and kept at 20 ± 2 °C during the
181 measurements. The scattering intensity was corrected for the empty cell contribution, transmission,
182 and detector efficiency and was normalized to the absolute scale by direct measurement of the
183 intensity of the incident neutron beam. The integration of the normalized 2D intensity distribution
184 with respect to the azimuthal angle yielded the 1D scattering intensity distribution, $I(q)$, in cm^{-1}. The
185 reduction of the data was performed using standard BENSC procedures for small-angle isotropic
186 scattering. The background from the incoherent scattering coming from each sample was determined
187 from analysis of the Porod asymptotic limit and subtracted from the normalized spectra.
188 Experimental data normalized to absolute scale were fitted using Igor routines (NCNR_SANS_
189 package_6.011) (Kline, 2006) available from NIST, National Institute for Standard and Technology,
190 Gaithersburg, MD, running on Igor Pro© (Wavemetric Inc., Lake Oswego, Oregon; Version 6.22).

191

192 **2.7. NSF/polymer interaction experiments**

193 2.7.1. Immersion tests

194 The aim of these tests was to investigate the direct interaction between cleaning fluids and polymer
195 films, without the influence of a medium (i.e., cellulose pulp poultice or gel). To this purpose, the
196 coated specimens were partly immersed in 32 ml of the selected fluids. The area of the polymer film
197 exposed to the fluid action was kept constant and fixed to 1×5 cm^2. At selected time intervals, up to
198 10 minutes, the specimens were extracted from the fluid and let dry, and then visual inspection of
199 possible changes in the film was carried out. At t = 0 min and t =10 min the superficial
200 micromorphology of the films (after drying) was investigated by optical microscopy and FTIR 2D
201 micro-reflectance mapping. Finally, after 10 min of incubation with each liquid system, a removal
202 test was performed on all the samples, using a cotton swab soaked with water, in order to check the
203 removability of the polymeric coatings.

204

205 2.7.2. Confocal laser scanning microscopy (CLSM)

206 Confocal Microscopy experiments were performed on a Leica TCS SP8 confocal microscope (Leica
207 Microsystems GmbH, Wetzlar, Germany) equipped with a 63x water immersion objective. The four
208 polymers were stained with Coumarin 6, which was dissolved/dispersed in the liquid solutions or
209 latexes. Then, 2-4 μm-thick polymer films were obtained by spin coating coverglasses for 60 s at
210 1000 rpm. Coumarin 6 was excited with the 488 nm laser line of an argon laser. The emission of the
211 dye was acquired with a PMT in the range 498–530 nm. CLSM experiments were performed to
212 monitor the interaction of the different polymer films with the NSF. Briefly, 50 μl of the unlabeled
213 liquid phase were put in contact with the coumarin 6–labeled polymer coated coverglass, and the
214 morphological variations of the polymeric film were monitored over time.

215

216 2.7.2. Cleaning tests

6

217 Two sets of cleaning tests were performed, in order to evaluate the influence on the application
218 method of the NSF, and the effect of the supporting material (i.e., cellulose pulp poultice or chemical
219 hydrogel) on the interaction between the NSF and the polymeric coating. Traditional cellulose pulp
220 poultices were prepared by mixing 35 mg of cellulose pulp (Arbocel®, Zecchi, Firenze) and 160 µl
221 of NSF. The obtained poultices were applied, interposing a Japanese paper sheet (Zecchi, Firenze)
222 between the compress and the specimen surface, on 1 cm^2 areas of each sample for 15 min. After
223 removing the poultices, a gentle mechanical action was performed on the treated surface, by means of
224 wet cotton swabs. Poly(hydroxyethyl methacrylate/poly vinylpyrrolydone) semi-interpenetrated
225 networks (pHEMA/PVP SIPNs) are highly retentive hydrogels, previously proposed in combination
226 with NSFs for the cleaning of works of art (Baglioni et al., 2018a), and prepared as described
227 elsewhere (Domingues et al., 2013a, 2013b). Gels having a size of $1 \times 1 \times 0.2$ cm^3 were used, able to
228 upload ca. 160 µl of NSF, i.e., the same amount of cleaning fluid loaded in the poultices. The gel was
229 applied for 15 min, and at the end of the treatment a gentle mechanical action was performed on the
230 coating residues.

231

2.8. Contact angle measurements

233 The contact angle of 5 µL sessile droplets of Milli-Q water on the selected material surface was
234 measured with a Rame-Hart Model 190 CA Goniometer. The three substrates and the four polymer
235 films were investigated. The equilibrium contact angle was measured in at least eight different areas,
236 and the average value and standard deviation was evaluated.

237

2.9. Optical microscopy

239 A Reichert Zatopan 353–890 microscope was used to collect micrographs. The instrument was
240 coupled with a Nikon Digital Sight DS-Fi2 camera. The NIS-ELEMENTS software was used to
241 capture and edit images.

242

2.10. Fourier-transform infrared spectroscopy – 2D Micro-reflectance mapping

244 The Fourier transform infrared (FTIR) 2D imaging of the treated surfaces was carried out using a
245 Cary 620-670 FTIR microscope, equipped with an FPA 128 ×128 detector (Agilent Technologies).
246 The spectra were recorded directly on the surface of the samples in reflectance mode, with open
247 aperture and a spectral resolution of 8 cm^{-1}, acquiring 128 scans for each spectrum. Each analysis
248 produces an IR map of 700×700 µm^2 (128 ×128 pixels), with a spatial resolution of 5.5 µm (i.e.
249 each pixel has dimensions of 5.5×5.5 µm^2 and is associated to an independent spectrum). In each
250 map, the intensity of a characteristic peak of each polymer, e.g. the C=O ester stretching typical of
251 both acrylics and vinyls, at about 1730 cm^{-1}, was shown with a chromatic scale, following the order
252 red > yellow > green > blue.

253

3. Results and discussion

255 **3.1. Polymer films characterization**

256 The four polymeric coatings were characterized by means of FTIR-ATR and contact angle
257 measurements. **Table 2** reports the values for the contact angle of water droplets laid on the surface
258 of the polymer films, or of the selected substrates (glass, marble, polystyrene). The substrates exhibit
259 a range of contact angles passing from hydrophilic (glass) to hydrophobic surfaces (polystyrene).
260 Regarding the polymers, it can be noticed that the acrylics are more hydrophobic than the vinyls, and
261 the films deriving from polymer latexes are more hydrophilic than those coming from solutions. This
262 is likely due to the presence of surfactants, stabilizers and other polar additives in the latexes
263 emulsions, which affect the wettability of the film.

264 **Table 2.** Contact angle of water droplets on the surface of the four selected polymeric coatings, and of the three types of
265 substrates.

| Sample	Contact angle	Substrate	Contact angle
V_S	$57.8 \pm 0.8°$	glass	$35.3 \pm 3.1°$
V_E	$39.1 \pm 1.9°$	marble	$61.7 \pm 1.8°$
A_S	$78.2 \pm 3.1°$	polystyrene	$77.0 \pm 1.6°$
A_E	$62.5 \pm 2.1°$		

266

267 **Figure 1** shows the FTIR-ATR spectra of the four polymer films. The spectra of the two vinyl films
268 match closely, confirming that the same type of polymers is present in both films. The main bands
269 were assigned as follows (Doménech-Carbó et al., 2001; Learner and Institute, 2004): C-H stretching
270 (2928 cm^{-1} and a shoulder at 2972 cm^{-1}); C=O stretching (intense and narrow peak at 1727 cm^{-1});
271 asymmetric stretching of the C-O group (1222 cm^{-1}, distinctive of PVAc); C-H in-plane bending
272 (1428 cm^{-1} and 1371 cm^{-1}); C-H out-of-plane bending (1117 cm^{-1}); C-O symmetric stretching (1018
273 cm^{-1}); C-C stretching (944 cm^{-1}); C-H rocking (792 cm^{-1}). Besides, the spectrum of V_E shows a broad
274 band at 3335 cm^{-1}, which is likely due to the OH stretching of poly(vinyl alcohol) (PVA), i.e., one of
275 the main additives of the Vinavil NPC® aqueous latex.

276

277

278

279

8
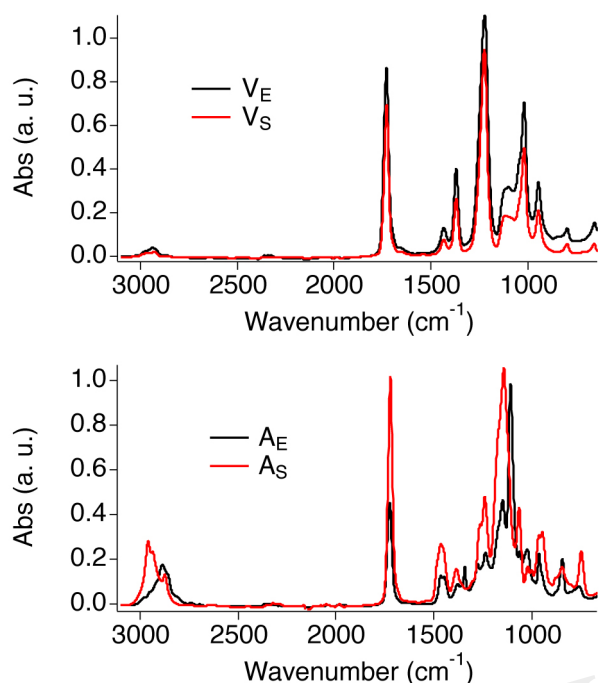
281   **Figure 1.** ATR spectra of the four polymeric films selected.

283   The spectra of A_S and A_E show slightly different features in the fingerprint and CH stretching
284   regions, as expected given the different type of acrylate polymers found in those films.

285   The main bands of the acrylic films were assigned as follows(Doménech-Carbó et al., 2001; Learner
286   and Institute, 2004; Pintus and Schreiner, 2011): C-H stretching (A_S: peaks at 2958, 2933, 2873 cm^{-1};
287   A_E: peaks at 2887 cm^{-1} and 2860 cm^{-1}); C=O stretching (1720 cm^{-1}); C-H in-plane bending (1465 and
288   1380 cm^{-1}; A_E shows an additional peak is visible at 1343 cm^{-1}); C-O stretching (A_S: peaks at 1240
289   and 1065 cm^{-1}; A_E: peaks at 1279, 1241, 1109, and 1022 cm^{-1}); C-C stretching (965 and 946 cm^{-1});
290   C-H rocking (840 and 750 cm^{-1}).

292   **3.2. NSF Characterization**

293   The selected NSF for this work is composed of water, a nonionic surfactant and two solvents, i.e.,
294   BuOH and MEK, which are partly miscible with water. The structure of this NSF was never studied
295   before, thus acquiring information on the micelles' size and shape, and on the location of each
296   component in the NSF, was deemed a preliminary step to help understanding the interaction of the
297   fluid with the polymeric films. To this aim, SANS measurements were performed on four D_2O based
298   samples: 1) the $D_2O/C_{9-11}E_{5.5}$ binary mixture; 2) the $D_2O/C_{9-11}E_{5.5}/BuOH$ ternary system; 3) the
299   complete NSF formulation, i.e., $D_2O/C_{9-11}E_{5.5}/BuOH/MEK$; 4) the complete NSF formulation with
300   deuterated d-MEK fully replacing the regular MEK. The analysis of samples 3 and 4 represents a
301   contrast variation experiment, in which everything is kept constant from one sample to the other,
302   except for its contrast, by changing the SLD of one or more chemicals (in this case, exchanging MEK
303   with d-MEK).

304   **Figure 2-top** shows the SANS profiles for the four samples analyzed. The data were fitted according
305   to two different models. The supramolecular aggregates, in the case of the binary surfactant/water
306   and the water/surfactant/BuOH systems, were modeled as non-interacting polydisperse core-shell
307   spheres, defined by two contrasts, *i.e.* bulk/shell and shell/core. On the other hand, the best fitting for
308   the complete NSF was obtained by modeling the micelles as non-interacting prolate core-shell
309   ellipsoidal particles, again defined by a double contrast. The scattering length density (SLD) of bulk,
310   shell and core, i.e., respectively, ρ_{bulk}, ρ_{shell} and ρ_{core}, were calculated according to the SLD for
311   neutrons of each chemical included in the formulations, as reported in **Table 3**. For globular micelles
312   of homogeneous scattering length density, the total scattered intensity $I(q)$ (cm^{-1}) is given by (Liu et
313   al., 1995; Sheu and Chen, 1988):

314    $$I(q) = N_P V_P^2 \Delta\rho^2 P(q) S(q) + \mathrm{bkg}_{inc} \qquad (1)$$

315   where N_p is the number density of the scattering particles (cm^{-3}), V_p is the volume (cm^3), $\Delta\rho$ is the
316   contrast term (cm^{-2}), $P(q)$ is the form factor and $S(q)$ is the structure factor. In this case $S(q) = 1$, as
317   the particles were considered to be non-interacting. In the case of spherical core-shell aggregates, the
318   particle scattering intensity is expressed as follows(Kline, 2006):

319    $$I(q) = \frac{\phi}{V_P}\left[(\rho_{core} - \rho_{shell}) \frac{3V_c j(qr_c)}{qr_c} + (\rho_{shell} - \rho_{bulk}) \frac{3V_P j(qr_s)}{qr_s} \right]^2 \qquad (2)$$

320   where $j(x)$ is a spherical Bessel function and is expressed as:

321    $$j(x) = \frac{(\sin x - x \cos x)}{x^2} \qquad (3)$$

322   and where ϕ is the volume fraction of the micellar phase, V_c is the core volume, r_c is the core radius,
323    $r_s = r_c + t$ (t is the shell thickness). Since this model takes into account a polydisperse core, which
324   follows the Schultz distribution, the form factor calculated in equation (2) is normalized by the
325   average particle volume:

326    $$\langle V \rangle = \frac{4\pi}{3} \langle r_c^3 \rangle \qquad (4)$$

327   where:

328    $$\langle r_c^3 \rangle = \frac{(z+2)(z+3)}{(z+1)^2} \langle r_c \rangle \qquad (5)$$

329   and z is the width parameter of the Schultz distribution(Degiorgio et al., 1985):

330    $$z = \frac{1}{\left(\frac{\sigma}{\langle r_c \rangle}\right)^2} - 1 \qquad (6)$$

331   being σ^2 the variance of the distribution. The polydispersity index (PDI), reported in **Table 4** is
332   defined as $\sigma/\langle r_c \rangle$ (see equation (6)) and its value is comprised between 0 and 1.

333   In the case of monodisperse non-interacting prolate ellipsoids, on the other hand, when modeling
334   asymmetric micelles with a core-shell scattering length profile, $P(q)$ included in equation (1) is
335   usually calculated as an orientationally-averaged normalized form factor, $\bar{P}(q)$. First, the orientation-

336 dependent form factor $F(q,\mu)$, is defined as follows (where μ is the cosine between the direction of
337 the symmetry axis of the ellipsoid and the Q vector):

338 $$F(q,\mu) = f(\rho)\frac{3j(u)}{u} + (1 - f(\rho))\frac{3j(v)}{v} \qquad (7)$$

339 where $j(x)$ is the same spherical Bessel function defined in eq. (3) and u and v are expressed as:

340 $$u = q[\mu^2 a^2 + (1 - \mu^2)b^2]^{1/2} \qquad (8)$$

341 $$v = q[\mu^2(a + t)^2 + (1 - \mu^2)(b + t)^2]^{1/2} \qquad (9)$$

342 which define the geometrical shape of the micelles, and where $f(\rho)$ contains the contrast calculation,
343 and a, b, t are the geometrical parameters of the ellipsoid, i.e. the major semi-axis, the minor semi-
344 axis, and the shell thickness, respectively.

345 $\bar{P}(q)$ is then calculated as follows(Kotlarchyk and Chen, 1983):

346 $$\bar{P}(q) = \int_0^1 d\mu |F(q,\mu)|^2 \qquad (10)$$

347

348 **Table 3.** SLD for neutrons scattering of the chemicals included in the NSF.

Chemical formula/structure	Compound/molecular group	SLD (10^{-6} Å^{-2})
D_2O	Heavy water	6.39
$CH_3(CH_2)_{8-10}(OCH_2CH_2)_{5.5}OH$	$C_{9-11}E_{5.5}$[a]	0.37
$CH_3(CH_2)_{8-10}$[a]	$C_{9-11}E_{5.5}$ apolar tail	-0.41
$HO(CH_2CH_2O)_{5.5}$	$C_{9-11}E_{5.5}$ polar head	0.97
$C_4H_{10}O$	BuOH	-0.33
$C_4H_3D_5O$	d-MEK	3.66
C_4H_8O	MEK	0.17

349 [a]For the SLD calculation a C_{10} aliphatic chain was considered.

350

Figure 2. Top) SANS profiles of the four samples analyzed. The best fitting curves are represented as continuous black lines. Bottom) The cartoon illustrates the structural evolution (in scale) of the three formulations investigated, i.e., the binary water/surfactant mixture, the water/surfactant/alcohol system, and the complete NSF.
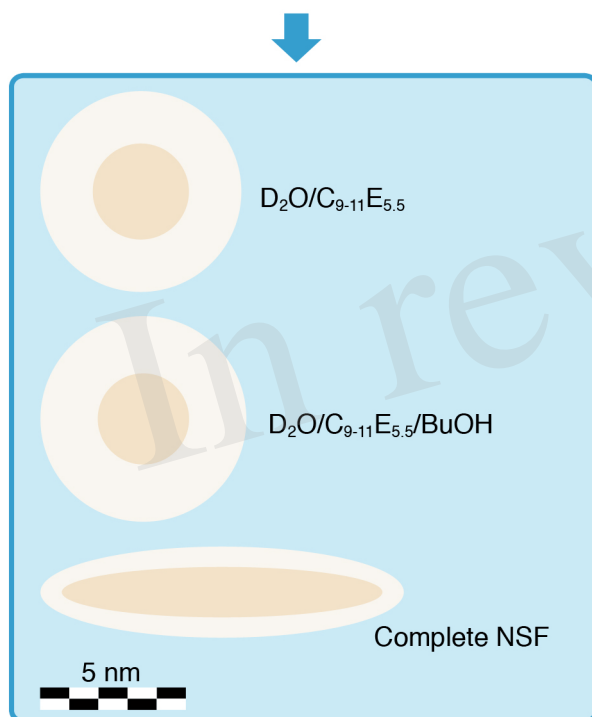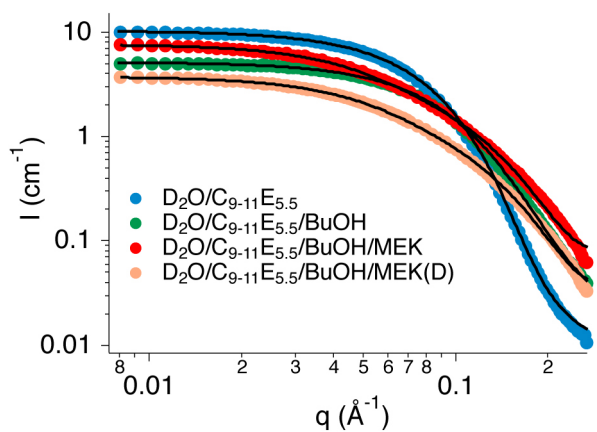
351

352 **Figure 2.** Top) SANS profiles of the four samples analyzed. The best fitting curves are represented as continuous black
353 lines. Bottom) The cartoon illustrates the structural evolution (in scale) of the three formulations investigated, i.e., the
354 binary water/surfactant mixture, the water/surfactant/alcohol system, and the complete NSF.

355

356 Even though the measured samples included D_2O instead of H_2O, the structural picture emerging
357 from the analysis of SANS data can be safely transferred to the H_2O-based NSF, apart from possible
358 slight changes (Baglioni et al., 2012a).

359 **Table 4** shows the main fitting results, while **Figure 2-bottom** contains a cartoon depicting the size
360 and shape evolution of micelles following the addition of each component to the formulation. The
361 size of $C_{9-11}E_{5.5}$ micelles in D_2O was perfectly consistent with the length of the surfactant molecule
362 and with the results of previous SAXS measurements performed on similar systems (Baglioni et al.,
363 2017), where a $r + t$ total micelle radius of about 35 Å had been obtained. A polydispersity index of
364 0.2 for the size of the hydrophobic core fits such systems, which usually have a PDI in the 0.1 - 0.5

12

365　range. According to fitting results, the structure and size of the micelles do not change significantly
366　after the addition of BuOH (see **Figure 2-bottom)**. In fact, BuOH was found to be partitioned
367　between the micellar and the aqueous bulk phase in a 30:70 ratio, meaning that most of the solvent is
368　mixed with water. The fraction solubilized in the micelles is preferentially located in the shell,
369　replacing D_2O hydration molecules, and thus affects the micellar size and shape only slightly. The
370　main effect of the inclusion of BuOH is to double the polydispersity of the core radius with respect to
371　the binary water/surfactant system, even though the value is perfectly suitable for a micellar solution.

372　The results of the contrast variation experiments performed on the complete NSF formulation
373　showed that the inclusion of a significant amount of MEK in the system completely alters both the
374　size and shape of the aggregates (see **Figure 2-bottom**), as the result of a sphere-to-rod transition.
375　This behavior was observed for similar systems containing the same surfactant (Baglioni et al., 2014)
376　and is likely due to the system getting closer to its cloud point. In fact, micelles are known to grow
377　and assume elongated shapes close to the clouding temperature, as observed in the present case. $C_{9-11}E_{5.5}$
378　has a cloud point of about 55-60 °C, which is known to be lowered by the interaction of this
379　surfactant with MEK (Baglioni et al., 2014). The inclusion of MEK in the system does not alter
380　significantly the partition coefficient of BuOH (P_{BuOH}) between the micelles and the water phase,
381　while MEK is mainly dissolved in the bulk phase (P_{MEK} = 0.17).

382　Overall, SANS analysis clarified that the structure of the NSF is that of rod-like micelles, mainly
383　composed of the sole surfactant, dispersed in a water/solvents mixture, indicating that the system is
384　close to its cloud point. This structural information has relevant implications in terms of cleaning
385　power of the NSF, as detergency is known to be maximized when these systems are close to the
386　cloud point (Baglioni et al., 2014; Holmberg, 2002; Holmberg et al., 2002; Stubenrauch, 2008).
387　Therefore, high cleaning effectiveness was expected from this NSF formulation.

388

389　**Table 4.** Fitting results of the SANS data acquired on the NSF.

Fitting parameter	$D_2O/C_{9-11}E_{5.5}$	$D_2O/C_{9-11}E_{5.5}$/BuOH	Complete NSF
r (Å)	16.7 ± 0.3	15.7 ± 0.2	-
t (Å)	17.9 ± 0.1	19.6 ± 0.1	9.4 ± 0.4
PDI	0.20 ± 0.01	0.40 ± 0.02	-
a (Å)	-	-	53.0 ± 2.0
b (Å)	-	-	7.2 ± 0.3
P_{BuOH}	-	0.30 ± 0.03	0.28 ± 0.02
P_{MEK}	-	-	0.17 ± 0.01

13

390

391

3.3. NSF/polymer interaction

The interaction between the NSF and the four polymer films was initially investigated simply by immersing the coated specimens into four different liquid systems, i.e., water, water/surfactant, water/solvents, and the complete NSF. The micromorphology of the film was observed by optical microscopy at different times during the total 10 minutes of incubation of the specimens in the liquids, while 2D micro-FTIR mapping was performed on the polymer surface before exposure to the fluids and after 10 minutes of incubation. Finally, a removal test was performed on the polymers using wet cotton swabs, in order to check their removability.

400

Table 5. Results of immersion tests performed on polymer-coated glass, marble and polystyrene specimens. Both the film appearance and its removability after 10 min of incubation in the four different liquid systems are summarized in the table, following analysis with optical microscopy and 2D micro-FTIR mapping.

		Glass		Marble		Polystyrene	
		Film appearance	Removability[a]	Film appearance	Removability[a]	Film appearance	Removability[a]
V_S	H_2O	No change	±	No change	x	No change	x
	$H_2O/C_{9-11}E_{5.5}$	Swollen	o	Swollen	±	Swollen	±
	$H_2O/BuOH/MEK$	Dewetted	o	Dewetted	o	Dewetted	o
	NSF	Dewetted	o	Dewetted	o	Dewetted	o
A_S	H_2O	No change	x	No change	x	No change	x
	$H_2O/C_{9-11}E_{5.5}$	Swollen	o	Swollen	x	Swollen	x
	$H_2O/BuOH/MEK$	Dewetted	o	Partly dewetted	±	Swollen	x
	NSF	Dewetted	o	Dewetted	o	Swollen	x
V_E	H_2O	Swollen	o	Swollen	o	Partly dewetted	o
	$H_2O/C_{9-11}E_{5.5}$	Swollen	o	Swollen	o	Partly	o

						dewetted	
	$H_2O/BuOH/MEK$	Swollen	o	Swollen	o	Swollen	±
	NSF	Swollen	o	Swollen	o	Partly dewetted	o
	H_2O	Swollen	o	Swollen	o	Swollen	o
	$H_2O/C_{9-11}E_{5.5}$	Swollen	o	Swollen	o	Swollen	o
A_E	$H_2O/BuOH/MEK$	Swollen	o	Swollen	o	Swollen	±
	NSF	Swollen	o	Swollen	o	Swollen	o

404 [a]After 10 min of incubation in the liquid systems, the removability of the coatings was checked performing a gentle
405 mechanical action with a cotton swab soaked with water; x = no removal, ± = partial removal, o = complete removal.

406

407 Looking at the results of the immersion tests, illustrated in **Figures 3- 6** and summarized in **Table 5**,
408 a clear difference in the behavior of samples emerges, i.e. the polymer films deriving from latexes
409 (V_E and A_E) are preferentially swollen and only in few cases partly dewetted, whereas the films
410 deriving from solutions are unaffected by just water, are swollen by the surfactant solution, and are
411 partly or completely dewetted when solvents are included in the liquid systems. For instance, **Figures
412 3 and 5** show how for chemically identical polymers (both PVAc) the type of the film plays a key
413 role in determining the behavior when the film is exposed to the same NSF. 2D microFTIR mapping
414 was crucial to confirm the location and distribution of the polymers on the micron-scale. In
415 particular, when a film is dewetted (see **Figures 3 and 4**) it was shown that no polymer residues are
416 present (above the instrumental detection limit) outside the droplets on the substrate surface.

417 Polymer coatings formed from aqueous emulsions are significantly more sensitive to the action of
418 water (a well known issue when emulsion-based acrylic paint layers are exposed to aqueous cleaning
419 fluids(Murray et al., 2002; Ormsby and Learner, 2009; Willneff et al., 2014)), and tend to be swollen.
420 This is justified by the presence of a non-negligible amount of hydrophilic additives and surfactants
421 in the polymer emulsions, which remain in the film after drying and are able to interact with water
422 molecules, favoring the swelling of the film. The presence of hydrophilic additives can also explain
423 why the swollen films tend to dewet less easily. The energetic balance of dewetting can be described
424 by the spreading coefficient S, which for a polymer film on a glass surface, immersed in a liquid, is
425 defined as (Baglioni and Chelazzi, 2013):

426 $$S = \gamma_{LG} - \gamma_{PG} - \gamma_{LP} \qquad (10)$$

427 where γ_{LG} is the interfacial tension between glass and the liquid, γ_{PG} is the interfacial tension between
428 glass and the polymer, and γ_{LP} is the interfacial tension between the liquid and the polymer. When S
429 is negative, dewetting is energetically favored and occurs spontaneously unless an activation energy
430 barrier hinders the process kinetically. Hydrophilic additives in the polymer film might lower the
431 values of both γ_{PG} and γ_{LP}, making S less negative for a given liquid/polymer/glass set. On the other

432   hand, the presence of surfactant additives may lower the glass transition temperature (T_g) of the
433   polymer films (as in the case of V_E – see Table 1), making polymer chains more mobile, thus
434   possibly decreasing the energy costs related to the formation of new interfacial regions during the
435   detachment of the film, and lowering the activation energy necessary to initiate dewetting (Baglioni
436   et al., 2017, 2018b; Montis et al., 2019).

437   Overall, in the case of the polymer films from emulsions investigated here, the films' thermodynamic
438   stability seems to prevail on the kinetic drive of the dewetting process. However, the swollen films
439   are softened and easily removable from glass and marble even with water and water/ $C_{9-11}E_{5.5}$,
440   meaning that the adhesion to the solid surface was sensibly reduced, while in the case of polystyrene
441   the removal is slightly more difficult. When a polymer film formed from a solvent solution is
442   exposed to a cleaning fluid, a more diversified behavior is observed. Water and water/ $C_{9-11}E_{5.5}$ are
443   partly or completely ineffective in removing the films. Instead, dewetting processes are induced by
444   water/solvents mixtures or, more efficiently, by the synergistic action of solvents and surfactants
445   (Baglioni et al., 2017, 207, 2018b; Gentili et al., 2012; Xu et al., 2012). This is clearly exemplified by
446   A_S on marble, where water alone produces no visible effects on the polymer. The nonionic surfactant
447   micellar solution is able to induce some swelling of the film, but not sufficient to grant its easy
448   removal. A water/solvents mixture, on the other hand, produces a partial dewetting pattern, and the
449   film can be partly removed using some mechanical action. This means that solvents are able to swell
450   the polymer to such an extent that the T_g is lowered below room temperature, starting the dewetting
451   process. However, it is only with the synergistic action of a surfactant, which lowers the interfacial
452   tension at the liquid/substrate and liquid/polymer interfaces, that dewetting proceeds further, leading
453   to easy and complete polymer removal. The substrate's chemical nature is a key factor. Increasing the
454   hydrophobicity of the substrate, the affinity of the polymer film with the substrate increases, leading
455   to less efficient polymer removal, culminating with the limit case of A_S on polystyrene, which
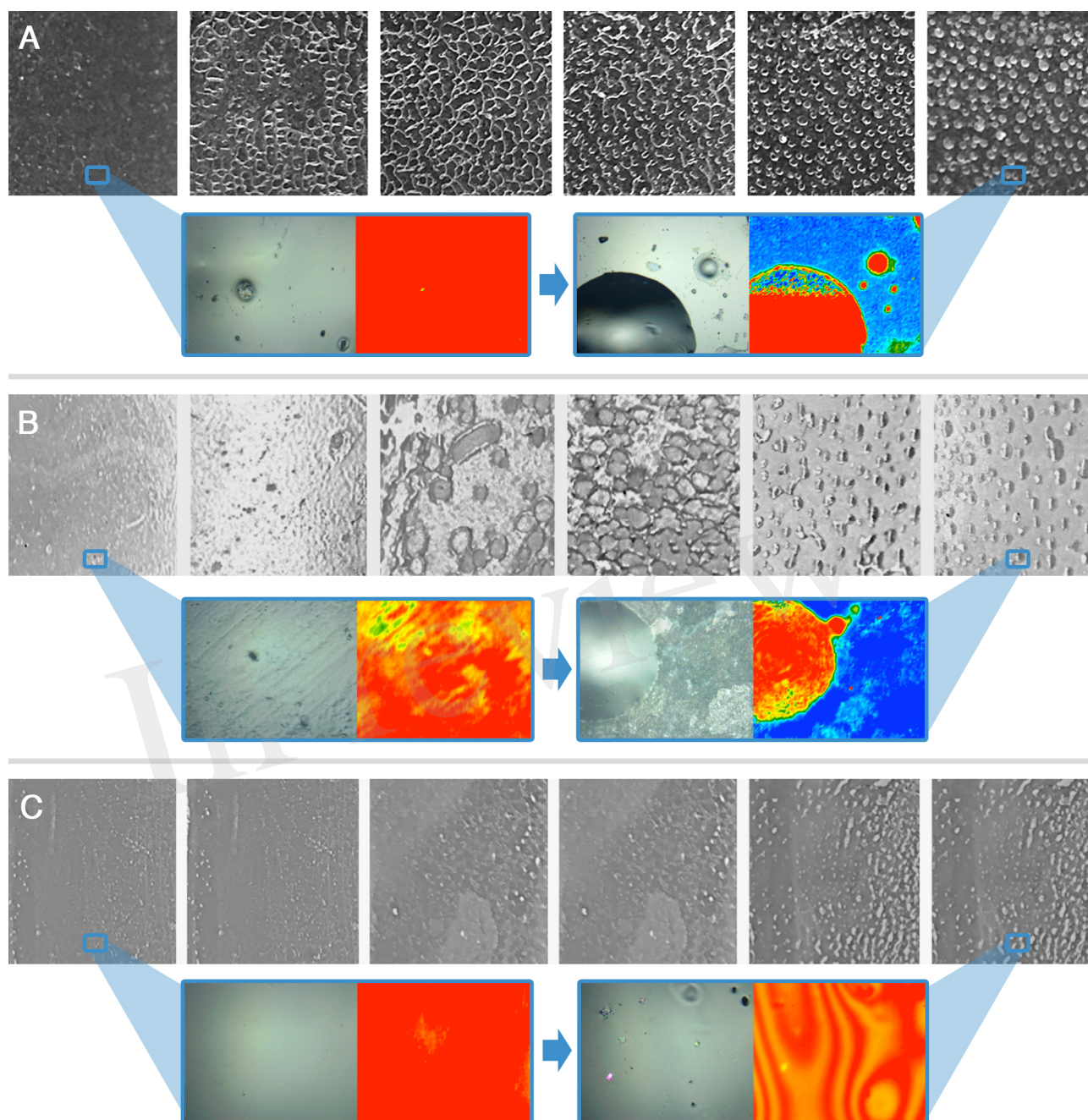456   resulted completely irremovable.

457

458
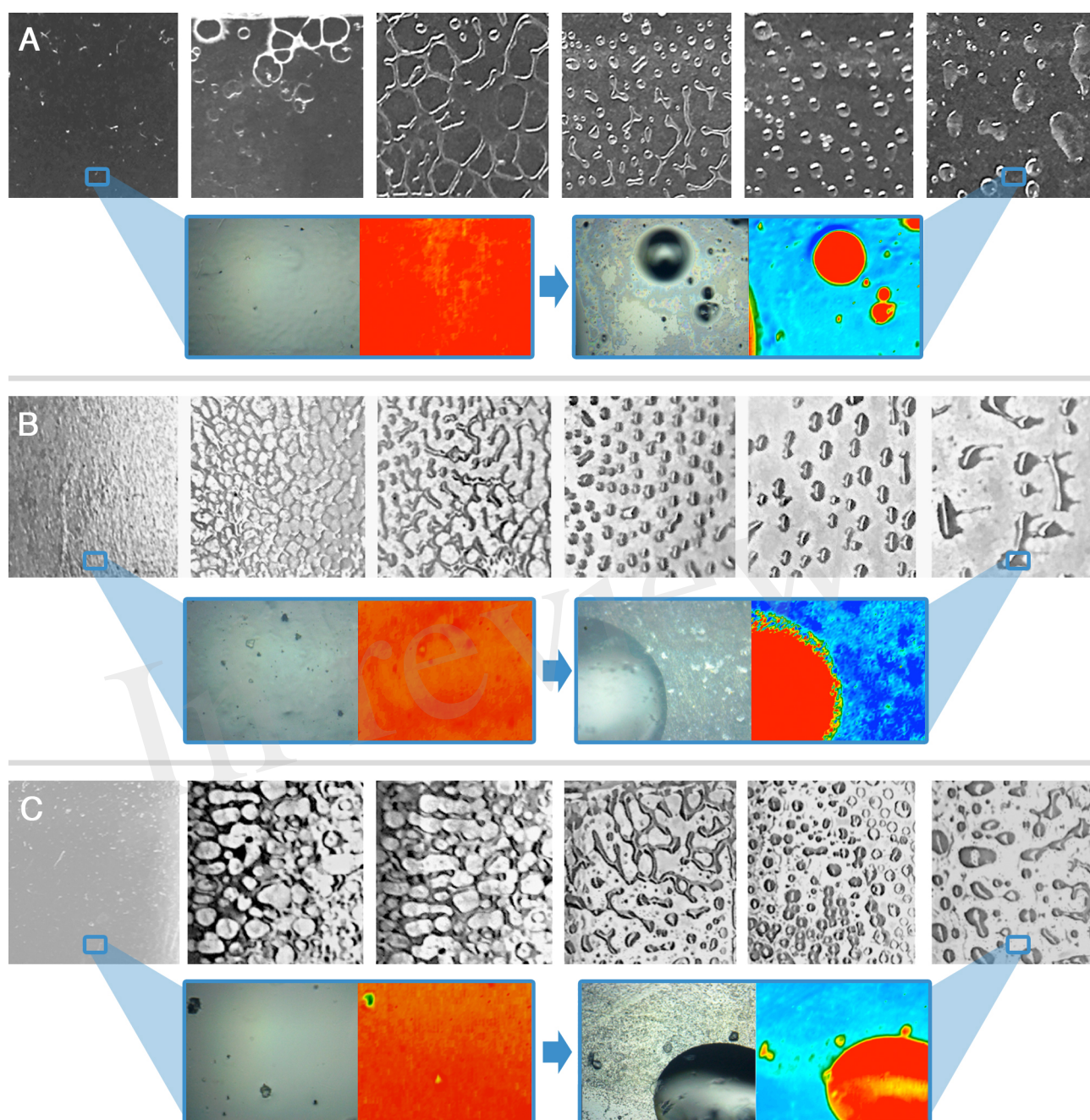
Figure 3. Immersion tests results for the V_S-coated glass (A), marble (B) and polystyrene (C) specimens. The frames, left to right, are taken at t = 0 s, 10 s, 30 s, 1 min, 5 min, 10 min. For t = 0 s and t =10 min a representative 2D micro-reflectance FTIR map is reported, together with its relative micrograph in visible light. In each map, the intensity of the C=O ester stretching at about 1730 cm^{-1} is shown with a chromatic scale, following the order red > yellow > green > blue. Visible light micrographs are approximately 1 cm^2 large; the FTIR mapping areas have a size of 400 μm × 550 μm.

464

465

466

Figure 4. Immersion tests results for the A$_S$-coated glass (A), marble (B) and polystyrene (C) specimens. The frames, left to right, are taken at t = 0 s, 10 s, 30 s, 1 min, 5 min, 10 min. For t = 0 s and t =10 min a representative 2D micro-reflectance FTIR map is reported, together with its relative micrograph in visible light. In each map, the intensity of the C=O ester stretching at about 1730 cm^{-1} is shown with a chromatic scale, following the order red > yellow > green > blue. Visible light micrographs are approximately 1 cm^2 large; the FTIR mapping areas have a size of 400 μm × 550 μm.
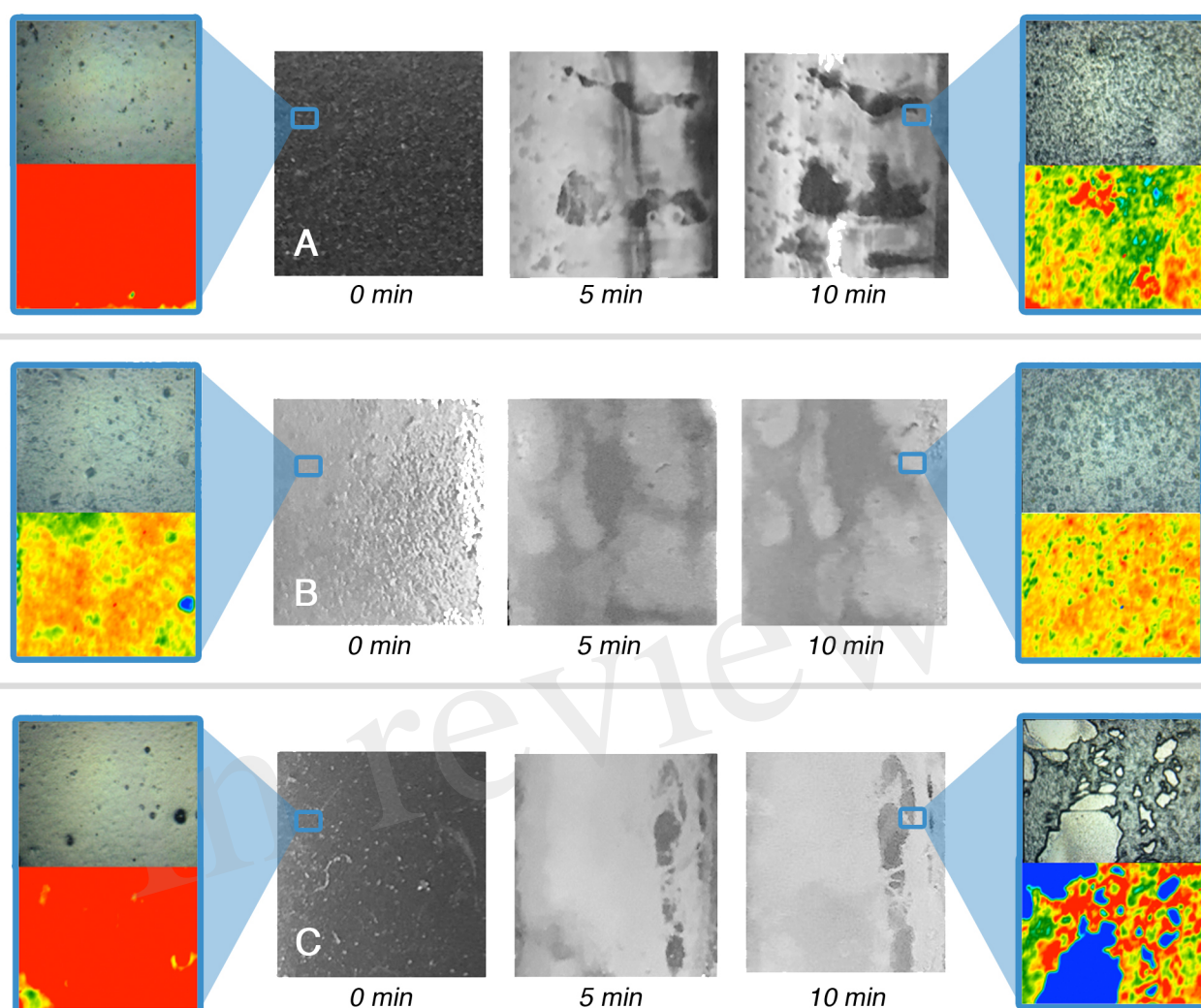
Figure 5. Immersion tests results for the V_E-coated glass (A), marble (B) and polystyrene (C) specimens. For t = 0 s and t =10 min a representative 2D micro-reflectance FTIR map is reported, together with its relative micrograph in visible light. In each map, the intensity of the C=O ester stretching at about 1730 cm^{-1} is shown with a chromatic scale, following the order red > yellow > green > blue. Visible light micrographs are approximately 1 cm^2 large; the FTIR mapping areas have a size of 400 µm × 550 µm.

485
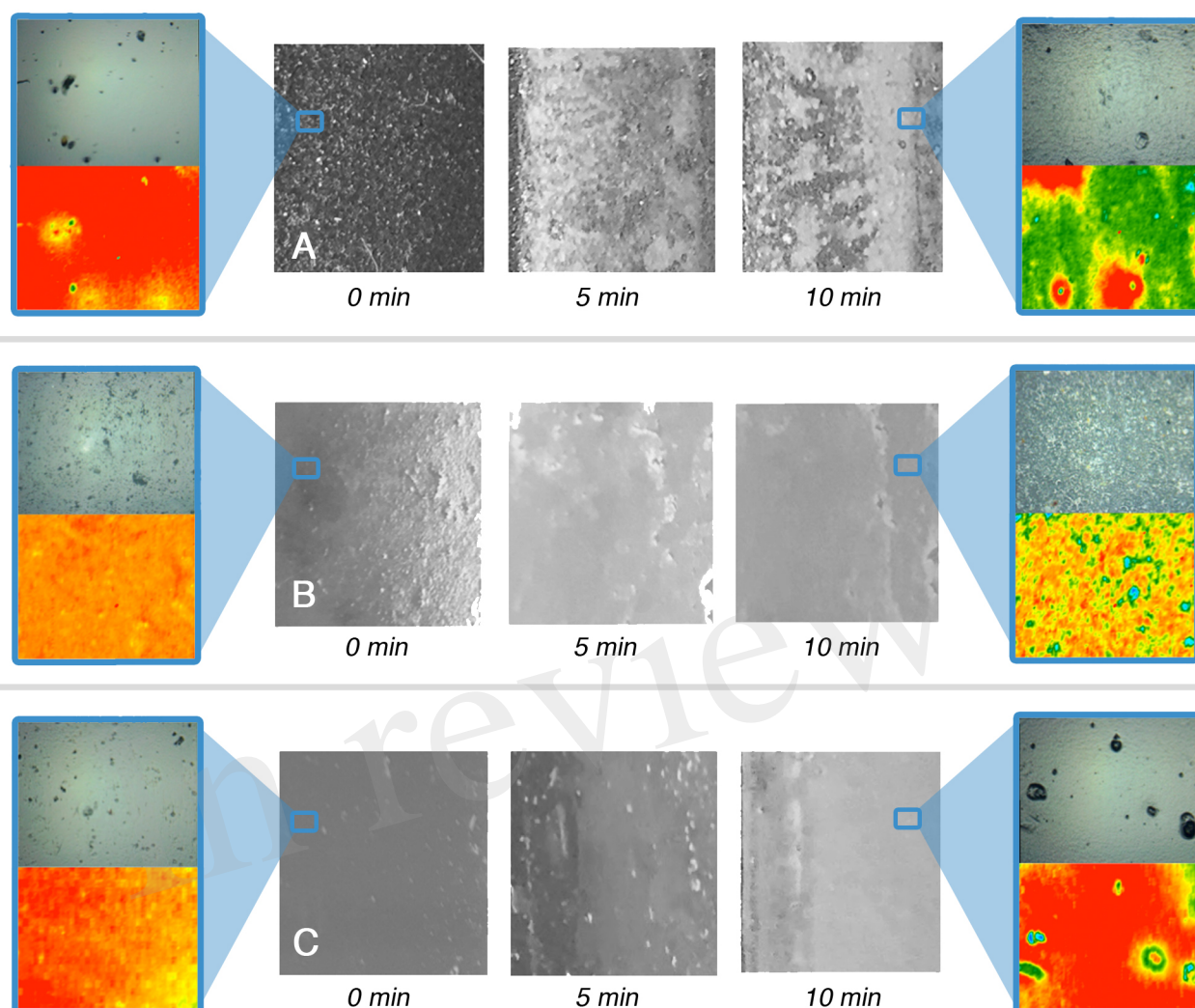
Figure 6. Immersion tests results for the A_E-coated glass (A), marble (B) and polystyrene (C) specimens. For t = 0 s and t =10 min a representative 2D micro-reflectance FTIR map is reported, together with its relative micrograph in visible light. In each map, the intensity of the C=O ester stretching at about 1730 cm^{-1} is shown with a chromatic scale, following the order red > yellow > green > blue. Visible light micrographs are approximately 1 cm^2 large; the FTIR mapping areas have a size of 400 µm × 550 µm.

491

The interaction between the complete NSF and the four polymer films was also monitored through CLSM imaging, as described in Section 2.7.2. Homogeneous and reproducible 2-4 µm thick films on coverglasses were obtained by spin coating. **Figure 7** summarizes the results of the investigation, which were in perfect agreement with what was observed during the immersion tests reported above. A_S and V_S, i.e. the polymer films cast from solutions, were completely and quickly dewetted by the NSF, while A_E and V_E, i.e. the films cast from polymer latexes, were just swollen. **Figure 7** shows that some small cracks and/or holes (of few microns) are visible in the V_E and A_E swollen films, which nonetheless maintain their overall coherence on a macro-scale. These holes possibly form in correspondence of previous film defects, which can be present on such thin films. Overall, the behavior of polymer films cast from aqueous latexes can be seen as the physical process stopped at the very early stages of dewetting. This is in agreement with what observed during previous

20

503 experiments, and seems to enforce the hypothesis that the amphiphilic additives in these films play a
504 key role in inhibiting the dewetting process, which otherwise would likely occur.

505 The inhomogeneous aspect of the V_E and A_E films at t = 0 is due to the fact that the hydrophobic
506 fluorescent dye was not evenly distributed in the aqueous polymer latex. As the films is swollen by
507 the penetration of the organic solvents, the dye evenly spread through the film.

508 CLSM investigations, overall, allowed to confirm the results of the immersion tests on macroscopic
509 samples, where the polymer thickness could not be directly measured and not accurately controllable.

510

511
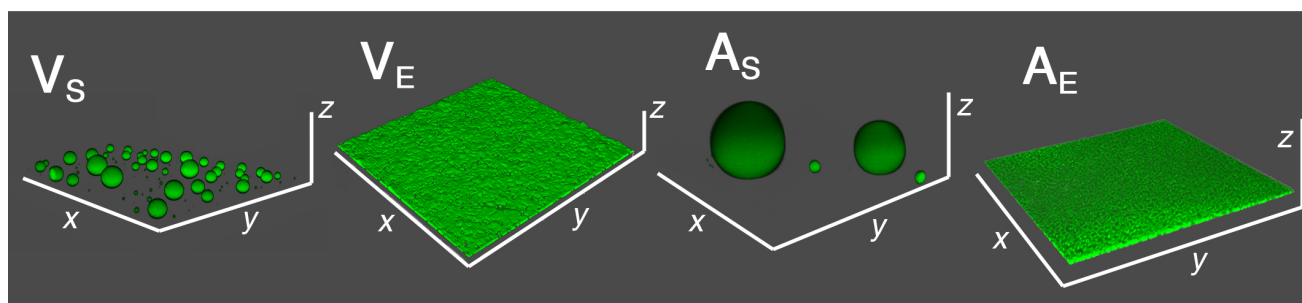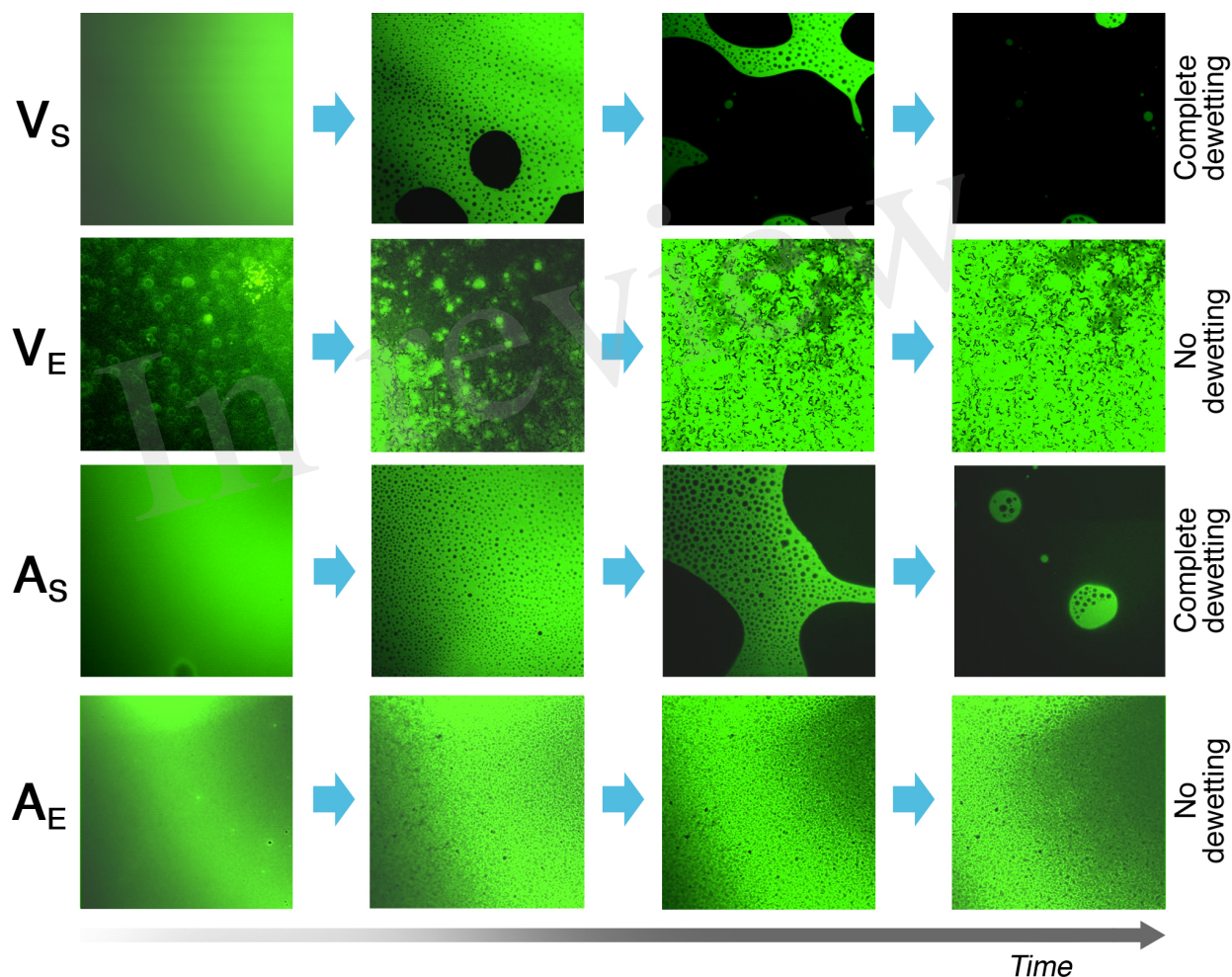
Figure 7. Results of CLSM experiments on 2-4 μm thick spin-coated polymer films on coverglasses. The films were exposed to the action of 50 μl of the complete NSF, and their morphology was observed over time. The time scale is not the same for all samples, i.e., V_S and A_S completely dewetted from the coverglass in less than 10 s, while V_E and A_E films were still intact after 10 minutes of incubation with the NSF. In the bottom grey box, the 3D reconstruction of the four polymers' morphology after 10 minutes is reported. The different behavior between polymer films coming from solvent solutions or aqueous emulsions is clearly evidenced. Each side of the CLSM micrographs is 150 μm long. *x* and *y* axes in the 3D reconstructions have the same length.

Finally, the influence of the application methodology on the outcome of removal tests was evaluated. To this aim, the same amount of NSF was uploaded respectively in traditional cellulose pulp poultices and in pHEMA/PVP chemical hydrogels. The latter have been characterized and assessed in the last years, and their use for the removal of unwanted materials from water-sensitive substrates has been thoroughly reported (Baglioni et al., 2018a; Bonelli et al., 2018; Domingues et al., 2013a). Recently, SAXS and rheology studies showed that these gels act as "sponges", able to load different NSFs without being altered or dramatically alter the properties of the fluids (Baglioni et al., 2018a).

The two systems were applied for 15 minutes on the surface of the films, and then micrographs of the treated area were taken before checking the coating removability via gentle mechanical action with a wet cotton swab. As visible in **Figure 8**, the areas treated with the NSF-loaded poultice are generally more inhomogeneous than the ones treated with the NSF-loaded hydrogel. Moreover, several cellulose fibers were spotted on the samples that were in contact with the poultice, indicating the permanence of paper or cellulose pulp residues on the treated areas. Dewetting patterns could be clearly highlighted in the areas of A_S on glass and marble treated with the NSF-loaded hydrogel, indicating a more controlled and reliable cleaning action. In any case, after the removal of either the compress or the gel, complete and easy removal could be obtained via a gentle mechanical action using wet cotton swabs, for all the specimens except A_S on polystyrene. In this case, the acrylic polymer could not be removed after 15 minutes of application of either the NSF-loaded poultice or hydrogel (**Figures 9A** and **9B**). We hypothesized that in this case the application time was too long, causing the migration of solvents through the AS coating up to the polymer/substrate interface, where they interacted with polystyrene creating a sort of joint or adhesion layer between the polymer and the substrate. This issue is easily overcome by using multiple applications of shorter length, assuming the confining matrix of the NSF is enough retentive to release gradually the uploaded fluid on short time scales, which is the case of the pHEMA/PVP gels. In fact, repeated shorter applications (2 +2 +2 minutes) of the NSF loaded in the hydrogel allowed complete removal of the coating (as confirmed by the 2D microFTIR mapping), while uneven polymer residues were left from the same application using cellulose poultices (see **Figures 9C-F)** The cartoon in **Figure 9** summarizes the removal process in the two cases: using the highly retentive hydrogel it is possible to perform a gradual action, which proceeds layer by layer, controlling the interaction of the NSF with the substrate. This approach was recently used to perform highly selective removal of overpaintings and vandalism (Giorgi et al., 2017).

22
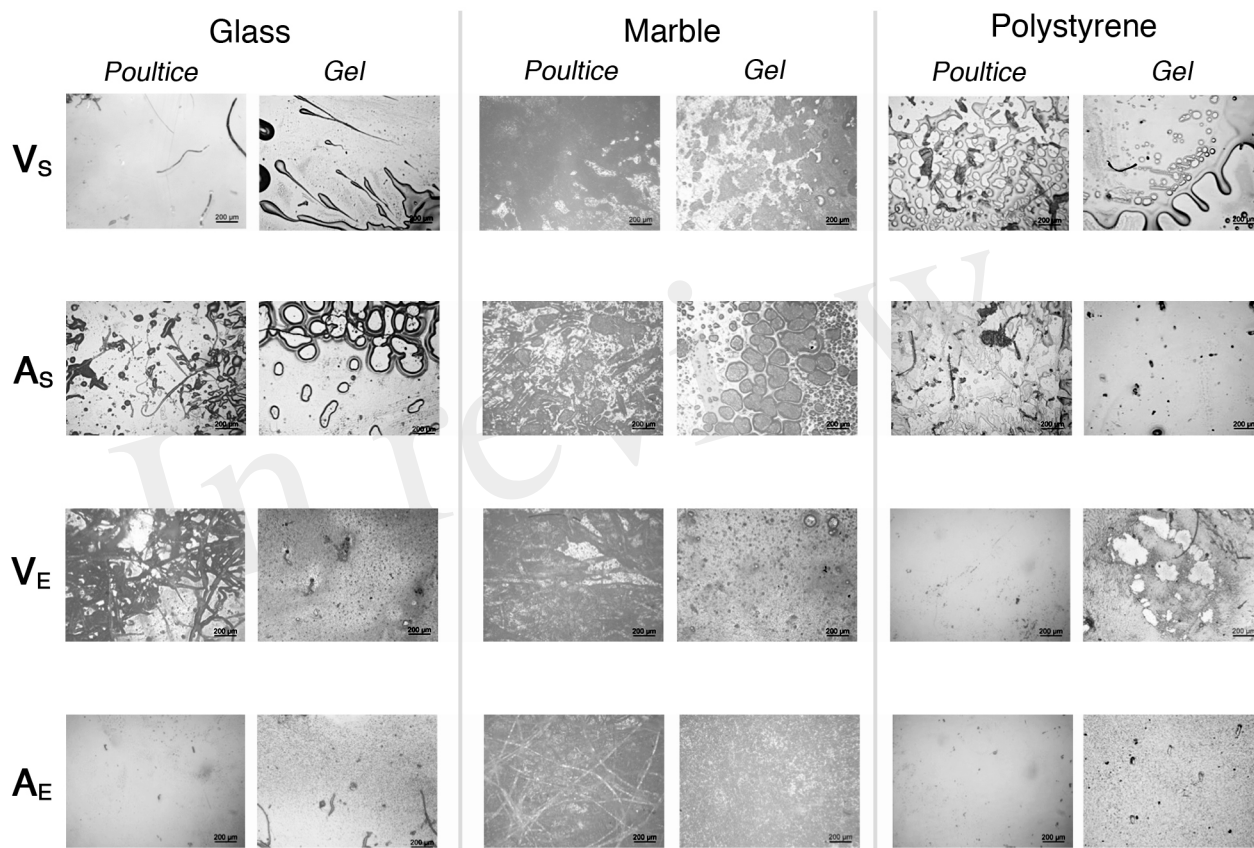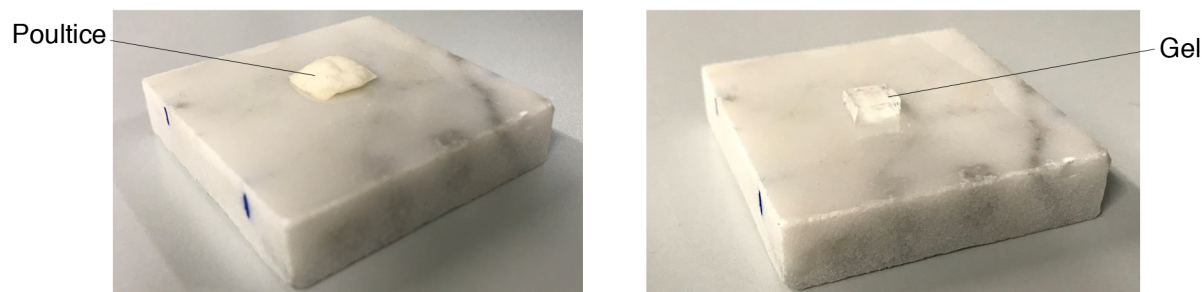
Figure 8. Results of the cleaning tests performed comparing the effect of the same amount of NSF loaded respectively on a traditional cellulose pulp poultice and on an innovative highly retentive chemical hydrogel. Top) Marble specimens during the tests. Bottom) Selected representative micrographs taken after 15 minutes of application of both the poultice and the gel. Each micrograph is 1.2×1.6 mm^2 large.

560
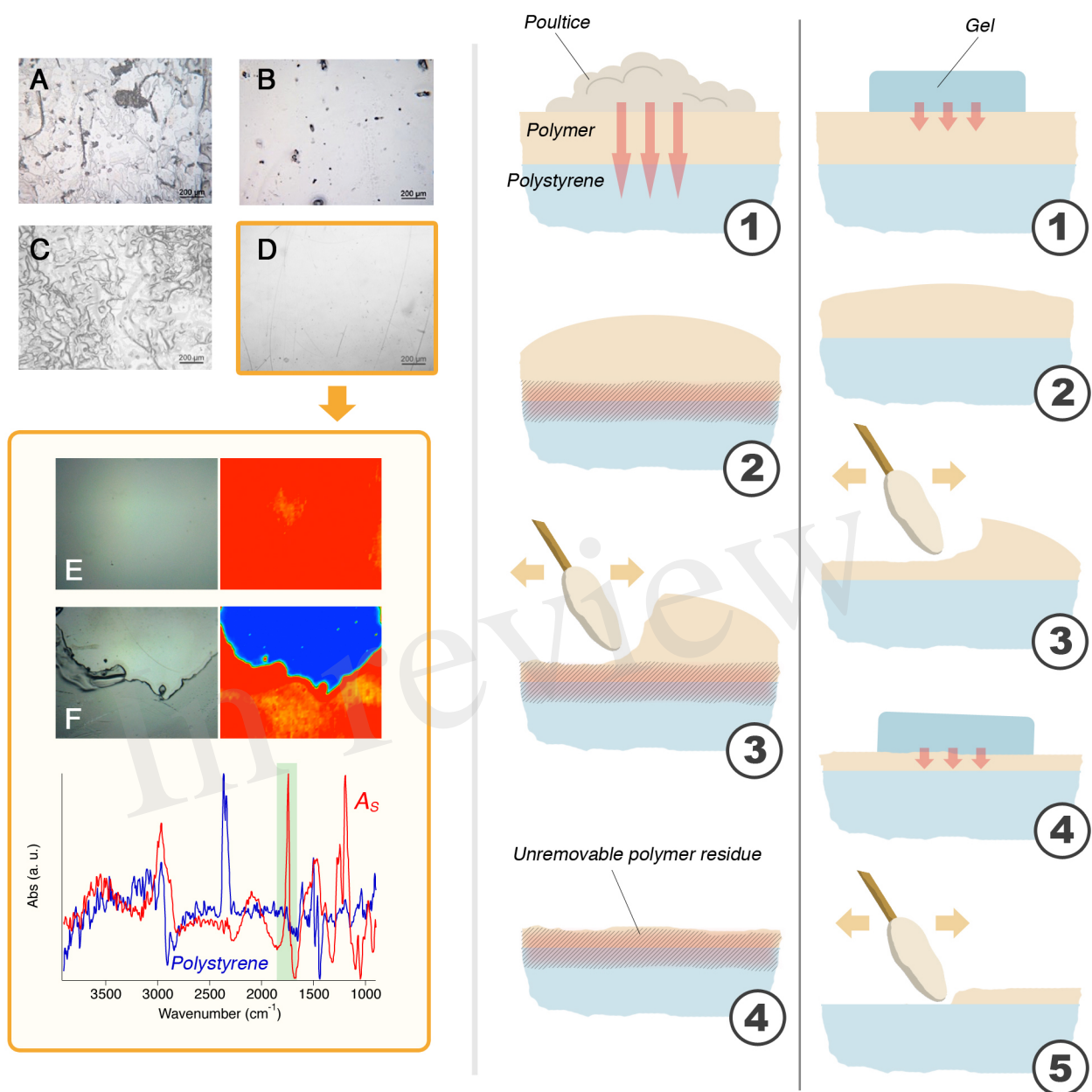
Figure 9. A) The result of 15 minutes of application of the NSF-loaded poultice on A_S laid on polystyrene; B) The result of 15 minutes of application of the NSF-loaded gel on A_S laid on polystyrene; C) The result of 2 min + 2 min + 2 min of application of the NSF-loaded poultice on A_S laid on polystyrene; D) The result of 2 min + 2 min + 2 min of application of the NSF-loaded gel on A_S laid on polystyrene. This is the only case that resulted in the complete removal of the polymer coating, as confirmed by the comparison between the micro-reflectance FTIR maps collected before (E) and after (F) the cleaning with the NSF-loaded hydrogel (the micro-picture is taken at the border between of the cleaned area, seen in blue). The cartoon on the right illustrates the mechanism proposed to explain the observed results. With the poultice (left), the solvents migrate through the polymer (1) and attack the polystyrene substrate, creating a junction or an enhanced adherence between the polymer film and the substrate (2). When a mechanical action is performed (3), an uneven layer of unremoved polymer layer is left stuck to the surface of polystyrene. Using the gel (right), the solvents migration is limited by the retention properties of the scaffold (1). The outer layers of the polymer coating are, then, slightly swollen (2) and easily removed by means of a gentle mechanical action (3). The gel is applied again (4) and the removal proceeds layer by layer, in a selective way, which allows for the complete and safe removal of the polymer film (5). Micrographs A, B, C and D are 1.2 × 1.6 mm² large; micrographs E and F (and relative FTIR maps) have a size of 400 μm × 550 μm.

576

577   **4. CONCLUSIONS**

578   This study focused on unveiling some key aspects of the NSFs/polymer coatings interaction
579   depending on several different factors: i) the chemical nature and, thus, hydrophilicity of the
580   substrate; ii) the chemical nature and physical structure of the polymeric films to be removed; iii) the
581   influence of the application methodology on the cleaning outcome. A series of systematic tests was
582   performed and a coherent and clear picture emerged. A water/$C_{9-11}E5.5$/BuOH/MEK NSF was
583   selected for this study and was firstly characterized by means of SANS measurements, which showed
584   that rod-like nonionic micelles are dispersed in a water/BuOH/MEK mixture close to the system
585   cloud point. These features possibly make this NSF particularly effective in polymer removal. Then,
586   glass, marble, and polystyrene specimens were coated with four different polymers, including two
587   vinyls and two acrylics, each applied either as a solvent solution or as an aqueous emulsion. It was
588   found that the NSF/polymer film interaction is greatly dependent on the film structure and
589   composition. Films formed from solvent solutions can be swollen by water/organic solvents mixtures
590   or dewetted when a surfactant is added to the cleaning fluid; films formed from polymer latexes, on
591   the other hand, are generally swollen even just by water, but they tend not to dewet. This happens
592   independently from the chemical nature of the polymer, and is a direct consequence of its structure
593   and composition, which includes a significant amount of amphiphilic additives. These substances
594   alter the energetic balance of the liquid/polymer/solid system and stabilize the film, which does not
595   dewet. However, these films are easily removable from the substrates, meaning that the action of the
596   cleaning fluid induces loss of adhesion, similarly to what happens during the first stages of the
597   dewetting process that occurs for films cast from polymer solutions. The substrate also plays an
598   important role in the removal of polymer films formed from solutions. In this case, the more the film
599   is affine to the substrate, the harder its removal. In the limit case, the removal of an acrylic polymer
600   from polystyrene could be achieved only through selective cleaning action using a NSF-loaded
601   highly retentive chemical hydrogel, which grants significantly more controlled performances than
602   traditional cellulose pulp poultices. These results have twofold relevance: they deepen the knowledge
603   of the physico-chemical processes that underpin phenomena of daily conservation practice, and
604   provide conservators with innovative solutions to face new challenges in art preservation.

605

606   **Conflict of Interest**

607   The authors declare that the research was conducted in the absence of any commercial or financial
608   relationships that could be construed as a potential conflict of interest.

609

610   **Author Contributions**

611   M.B, M.A., and D.C. contributed to the conception and design of the work, to the acquisition, the
612   analysis, and the interpretation of experimental data.

613   R.G. and P.B. revised the work critically giving a substantial intellectual contribution, and ultimately
614   provided the final approval for its publication.

615

626 **References**

627 Apostol, I., Damian, V., Garoi, F., Iordache, I., Bojan, M., Apostol, D., et al. (2011). Controlled
628   removal of overpainting and painting layers under the action of UV laser radiation. *Opt.*
629   *Spectrosc.* 111, 287. doi:10.1134/S0030400X11080054.

630 Baglioni, M., Bartoletti, A., Bozec, L., Chelazzi, D., Giorgi, R., Odlyha, M., et al. (2016).
631   Nanomaterials for the cleaning and pH adjustment of vegetable-tanned leather. *Appl. Phys. A*
632   122, 114. doi:10.1007/s00339-015-9553-x.

633 Baglioni, M., Berti, D., Teixeira, J., Giorgi, R., and Baglioni, P. (2012a). Nanostructured Surfactant-
634   Based Systems for the Removal of Polymers from Wall Paintings: A Small-Angle Neutron
635   Scattering Study. *Langmuir* 28, 15193–15202. doi:10.1021/la303463m.

636 Baglioni, M., Domingues, J. A. L., Carretti, E., Fratini, E., Chelazzi, D., Giorgi, R., et al. (2018a).
637   Complex Fluids Confined into Semi-interpenetrated Chemical Hydrogels for the Cleaning of
638   Classic Art: A Rheological and SAXS Study. *ACS Appl. Mater. Interfaces*.
639   doi:10.1021/acsami.8b01841.

640 Baglioni, M., Giorgi, R., Berti, D., and Baglioni, P. (2012b). Smart cleaning of cultural heritage: a
641   new challenge for soft nanoscience. *Nanoscale* 4, 42. doi:10.1039/c1nr10911a.

642 Baglioni, M., Jàidar Benavides, Y., Berti, D., Giorgi, R., Keiderling, U., and Baglioni, P. (2015a). An
643   amine-oxide surfactant-based microemulsion for the cleaning of works of art. *J. Colloid*
644   *Interface Sci.* 440, 204–210. doi:10.1016/j.jcis.2014.10.003.

645 Baglioni, M., Jáidar Benavides, Y., Desprat-Drapela, A., and Giorgi, R. (2015b). Amphiphile-based
646   nanofludis for the removal of styrene/acrylate coatings: Cleaning of stucco decoration in the
647   Uaxactun archeological site (Guatemala). *J. Cult. Herit.* 16, 862–868.
648   doi:10.1016/j.culher.2015.03.008.

649 Baglioni, M., Montis, C., Brandi, F., Guaragnone, T., Meazzini, I., Baglioni, P., et al. (2017).
650   Dewetting acrylic polymer films with water/propylene carbonate/surfactant mixtures –

26

651   implications for cultural heritage conservation. *Phys. Chem. Chem. Phys.* 19, 23723–23732.
652   doi:10.1039/C7CP02608K.

653 Baglioni, M., Montis, C., Chelazzi, D., Giorgi, R., Berti, D., and Baglioni, P. (2018b). Polymer Film
654   Dewetting by Water/Surfactant/Good-Solvent Mixtures: A Mechanistic Insight and Its
655   Implications for the Conservation of Cultural Heritage. *Angew. Chem. Int. Ed.* 57, 7355–
656   7359. doi:10.1002/anie.201710930.

657 Baglioni, M., Poggi, G., Ciolli, G., Fratini, E., Giorgi, R., and Baglioni, P. (2018c). A Triton X-100-
658   Based Microemulsion for the Removal of Hydrophobic Materials from Works of Art: SAXS
659   Characterization and Application. *Materials* 11, 1144. doi:10.3390/ma11071144.

660 Baglioni, M., Poggi, G., Jaidar Benavides, Y., Martínez Camacho, F., Giorgi, R., and Baglioni, P.
661   Nanostructured fluids for the removal of graffiti – A survey on 17 commercial spray-can
662   paints. *J. Cult. Herit.* doi:10.1016/j.culher.2018.04.016.

663 Baglioni, M., Raudino, M., Berti, D., Keiderling, U., Bordes, R., Holmberg, K., et al. (2014).
664   Nanostructured fluids from degradable nonionic surfactants for the cleaning of works of art
665   from polymer contaminants. *Soft Matter* 10, 6798–6809. doi:10.1039/C4SM01084A.

666 Baglioni, M., Rengstl, D., Berti, D., Bonini, M., Giorgi, R., and Baglioni, P. (2010). Removal of
667   acrylic coatings from works of art by means of nanofluids: understanding the mechanism at
668   the nanoscale. *Nanoscale* 2, 1723. doi:10.1039/c0nr00255k.

669 Baglioni, P., Berti, D., Bonini, M., Carretti, E., Del Carmen Casas Perez, M., Chelazzi, D., et al.
670   (2012c). Gels for the Conservation of Cultural Heritage. *MRS Online Proc. Libr.* 1418, null-
671   null. doi:10.1557/opl.2012.97.

672 Baglioni, P., Carretti, E., and Chelazzi, D. (2015c). Nanomaterials in art conservation. *Nat.*
673   *Nanotechnol.* 10, 287–290. doi:10.1038/nnano.2015.38.

674 Baglioni, P., and Chelazzi, D. (2013). *Nanoscience for the Conservation of Works of Art*. Royal
675   Society of Chemistry.

676 Bonelli, N., Montis, C., Mirabile, A., Berti, D., and Baglioni, P. (2018). Restoration of paper
677   artworks with microemulsions confined in hydrogels for safe and efficient removal of
678   adhesive tapes. *Proc. Natl. Acad. Sci.* 115, 5932–5937. doi:10.1073/pnas.1801962115.

679 Borgioli, L., Caminati, G., Gabrielli, G., and Ferroni, E. (1995). Removal of hydrophobic impurities
680   from pictorial surfaces by means of heterogeneous systems. *Sci. Technol. Cult. Herit. J. Of* 4,
681   67–74.

682 Burnstock, A., and Kieslich, T. (1996). A study of the clearance of solvent gels used for varnish
683   removal from paintings. in (London: James & James), 253–262.

684 Burnstock, A., and White, R. (2000). A preliminary assessment of the aging/degradation of
685   Ethomeen C-12 residues from solvent gel formulations and their potential for inducing
686   changes in resinous paint media.

687 Carretti, E., and Dei, L. (2004). Physicochemical characterization of acrylic polymeric resins coating
688   porous materials of artistic interest. *Prog. Org. Coat.* 49, 282–289.
689   doi:10.1016/j.porgcoat.2003.10.011.

690 Carretti, E., Dei, L., and Baglioni, P. (2003). Solubilization of Acrylic and Vinyl Polymers in
691   Nanocontainer Solutions. Application of Microemulsions and Micelles to Cultural Heritage
692   Conservation. *Langmuir* 19, 7867–7872. doi:10.1021/la034757q.

693 Carretti, E., Giorgi, R., Berti, D., and Baglioni, P. (2007). Oil-in-Water Nanocontainers as Low
694   Environmental Impact Cleaning Tools for Works of Art: Two Case Studies. *Langmuir* 23,
695   6396–6403. doi:10.1021/la700487s.

696 Chelazzi, D., Giorgi, R., and Baglioni, P. (2018). Microemulsions, Micelles, and Functional Gels:
697   How Colloids and Soft Matter Preserve Works of Art. *Angew. Chem. Int. Ed Engl.* 57, 7296–
698   7303. doi:10.1002/anie.201710711.

699 Chevalier, Y., Pichot, C., Graillat, C., Joanicot, M., Wong, K., Maquet, J., et al. (1992). Film
700   formation with latex particles. *Colloid Polym. Sci.* 270, 806–821. doi:10.1007/BF00776153.

701 Degiorgio, V., Corti, M., and fisica, S. italiana di (1985). *Physics of amphiphiles--micelles, vesicles,*
702   *and microemulsions: Varenna on Lake Como, Villa Monastero, 19-29 July 1983*. North-
703   Holland.

704 Doménech-Carbó, M. T., Doménech-Carbó, A., Gimeno-Adelantado, J. V., and Bosch-Reig, F.
705   (2001). Identification of Synthetic Resins Used in Works of Art by Fourier Transform
706   Infrared Spectroscopy. *Appl. Spectrosc.* 55, 1590–1602. doi:10.1366/0003702011954152.

707 Domingues, J. A. L., Bonelli, N., Giorgi, R., Fratini, E., Gorel, F., and Baglioni, P. (2013a).
708   Innovative Hydrogels Based on Semi-Interpenetrating p(HEMA)/PVP Networks for the
709   Cleaning of Water-Sensitive Cultural Heritage Artifacts. *Langmuir* 29, 2746–2755.
710   doi:10.1021/la3048664.

711 Domingues, J., Bonelli, N., Giorgi, R., and Baglioni, P. (2013b). Chemical semi-IPN hydrogels for
712   the removal of adhesives from canvas paintings. *Appl. Phys. A* 114, 705–710.
713   doi:10.1007/s00339-013-8150-0.

714 Gentili, D., Foschi, G., Valle, F., Cavallini, M., and Biscarini, F. (2012). Applications of dewetting in
715   micro and nanotechnology. *Chem. Soc. Rev.* 41, 4430–4443. doi:10.1039/C2CS35040H.

716 Giorgi, R., Baglioni, M., and Baglioni, P. (2017). Nanofluids and chemical highly retentive hydrogels
717   for controlled and selective removal of overpaintings and undesired graffiti from street art.
718   *Anal. Bioanal. Chem.*, 1–6. doi:10.1007/s00216-017-0357-z.

719 Giorgi, R., Baglioni, M., Berti, D., and Baglioni, P. (2010). New Methodologies for the Conservation
720   of Cultural Heritage: Micellar Solutions, Microemulsions, and Hydroxide Nanoparticles. *Acc.*
721   *Chem. Res.* 43, 695–704. doi:10.1021/ar900193h.

722 Holmberg, K. (2002). *Handbook of applied surface and colloid chemistry*. Wiley.

28

723 Holmberg, K., Jönsson, B., Kronberg, B., and Lindman, B. (2002). *Surfactants and Polymers in*
724 *Aqueous Solution*. Wiley.

725 Kavda, S., Richardson, E., and Golfomitsou, S. (2017). The Use of Solvent-Gel Systems for the
726 Cleaning of PMMA. *MRS Adv.* 2, 2179–2187. doi:10.1557/adv.2017.249.

727 Kline, S. R. (2006). Reduction and analysis of SANS and USANS data using IGOR Pro. *J. Appl.*
728 *Crystallogr.* 39, 895–900. doi:10.1107/S0021889806035059.

729 Kotlarchyk, M., and Chen, S.-H. (1983). Analysis of small angle neutron scattering spectra from
730 polydisperse interacting colloids. *J. Chem. Phys.* 79, 2461–2469. doi:10.1063/1.446055.

731 Learner, T., and Institute, G. C. (2004). *Analysis of Modern Paints*. Getty Publications.

732 Liu, Y. C., Ku, C. Y., LoNostro, P., and Chen, S. H. (1995). Ion correlations in a micellar solution
733 studied by small-angle neutron and x-ray scattering. *Phys. Rev. E* 51, 4598–4607.
734 doi:10.1103/PhysRevE.51.4598.

735 Montis, C., Koynov, K., Best, A., Baglioni, M., Butt, H.-J., Berti, D., et al. (2019). Surfactants
736 Mediate the Dewetting of Acrylic Polymer Films Commonly Applied to Works of Art. *ACS*
737 *Appl. Mater. Interfaces* 11, 27288–27296. doi:10.1021/acsami.9b04912.

738 Murray, A., Berenfeld, C. C. de, Chang, S. Y. S., Jablonski, E., Klein, T., Riggs, M. C., et al. (2002).
739 The Condition and Cleaning of Acrylic Emulsion Paintings. *MRS Online Proc. Libr. Arch.*
740 712. doi:10.1557/PROC-712-II1.4.

741 Ormsby, B., and Learner, T. (2009). The effects of wet surface cleaning treatments on acrylic
742 emulsion artists' paints – a review of recent scientific research. *Rev. Conserv.* 10, 29–41.

743 Pintus, V., and Schreiner, M. (2011). Characterization and identification of acrylic binding media:
744 influence of UV light on the ageing process. *Anal. Bioanal. Chem.* 399, 2961–2976.
745 doi:10.1007/s00216-010-4357-5.

746 Raudino, M., Giamblanco, N., Montis, C., Berti, D., Marletta, G., and Baglioni, P. (2017). Probing
747 the Cleaning of Polymeric Coatings by Nanostructured Fluids: A QCM-D Study. *Langmuir*
748 33, 5675–5684. doi:10.1021/acs.langmuir.7b00968.

749 Raudino, M., Selvolini, G., Montis, C., Baglioni, M., Bonini, M., Berti, D., et al. (2015). Polymer
750 Films Removed from Solid Surfaces by Nanostructured Fluids: Microscopic Mechanism and
751 Implications for the Conservation of Cultural Heritage. *ACS Appl. Mater. Interfaces* 7, 6244–
752 6253. doi:10.1021/acsami.5b00534.

753 Sanmartín, P., Cappitelli, F., and Mitchell, R. (2014). Current methods of graffiti removal: A review.
754 *Constr. Build. Mater.* 71, 363–374. doi:10.1016/j.conbuildmat.2014.08.093.

755 Sheu, E. Y., and Chen, S. H. (1988). Thermodynamic analysis of polydispersity in ionic micellar
756 systems and its effect on small-angle neutron scattering data treatment. *J. Phys. Chem.* 92,
757 4466–4474. doi:10.1021/j100326a044.

758 Steward, P. A., Hearn, J., and Wilkinson, M. C. (2000). An overview of polymer latex film formation
759   and properties. *Adv. Colloid Interface Sci.* 86, 195–267. doi:10.1016/S0001-8686(99)00037-
760   8.

761 Stubenrauch, C. (2008). *Microemulsions: Background, New Concepts, Applications, Perspectives*.
762   Wiley.

763 Verschueren, K. (2001). *Handbook of environmental data on organic chemicals*. Wiley.

764 Willneff, E. A., Schroeder, S. L., and Ormsby, B. A. (2014). Spectroscopic techniques and the
765   conservation of artists' acrylic emulsion paints. *Herit. Sci.* 2, 25. doi:10.1186/s40494-014-
766   0025-y.

767 Winnik, M. A. (1997). Latex film formation. *Curr. Opin. Colloid Interface Sci.* 2, 192–199.
768   doi:10.1016/S1359-0294(97)80026-X.

769 Xu, L., Sharma, A., and Joo, S. W. (2012). Dewetting of Stable Thin Polymer Films Induced by a
770   Poor Solvent: Role of Polar Interactions. *Macromolecules* 45, 6628–6633.
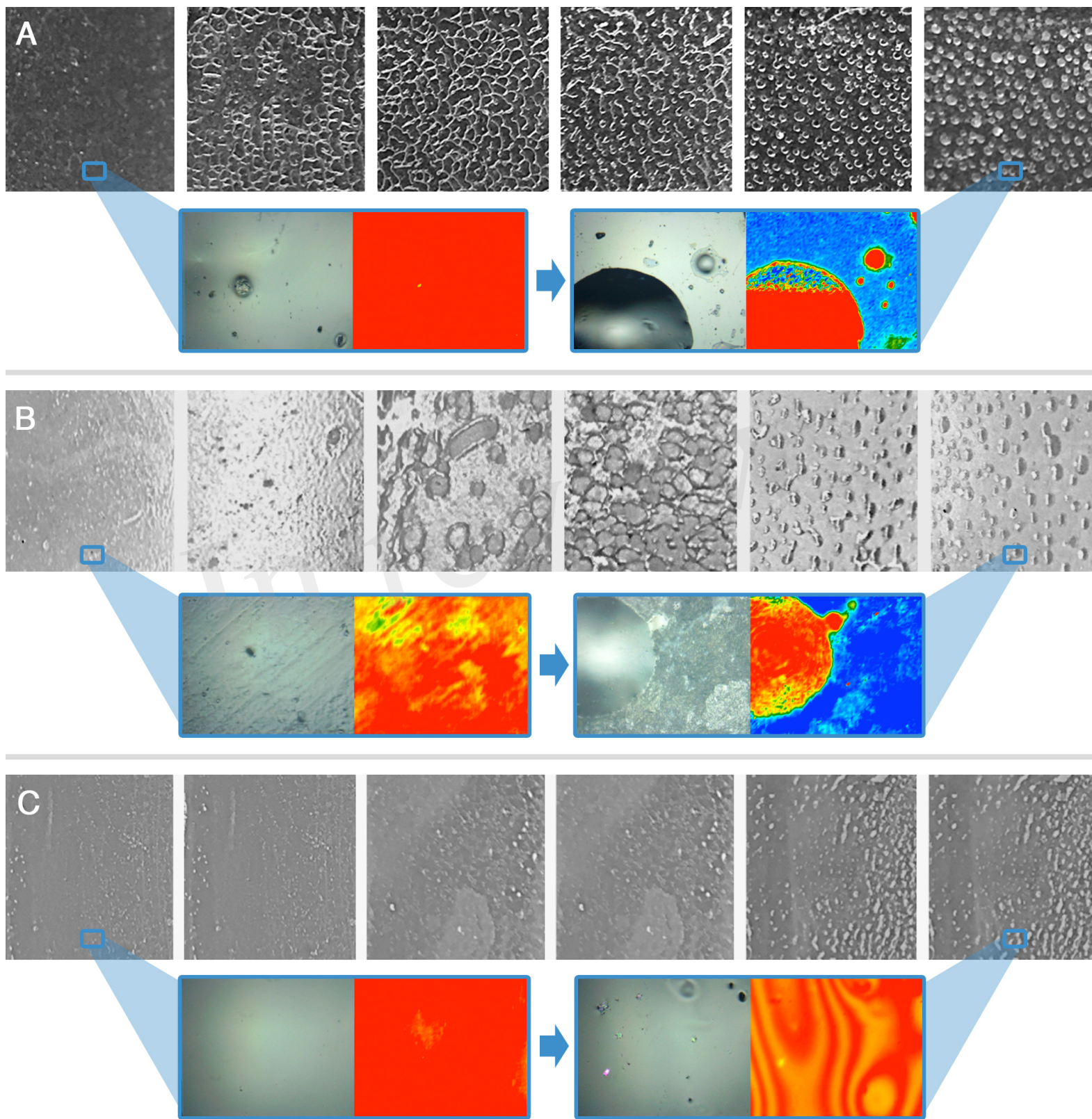771   doi:10.1021/ma301227m.
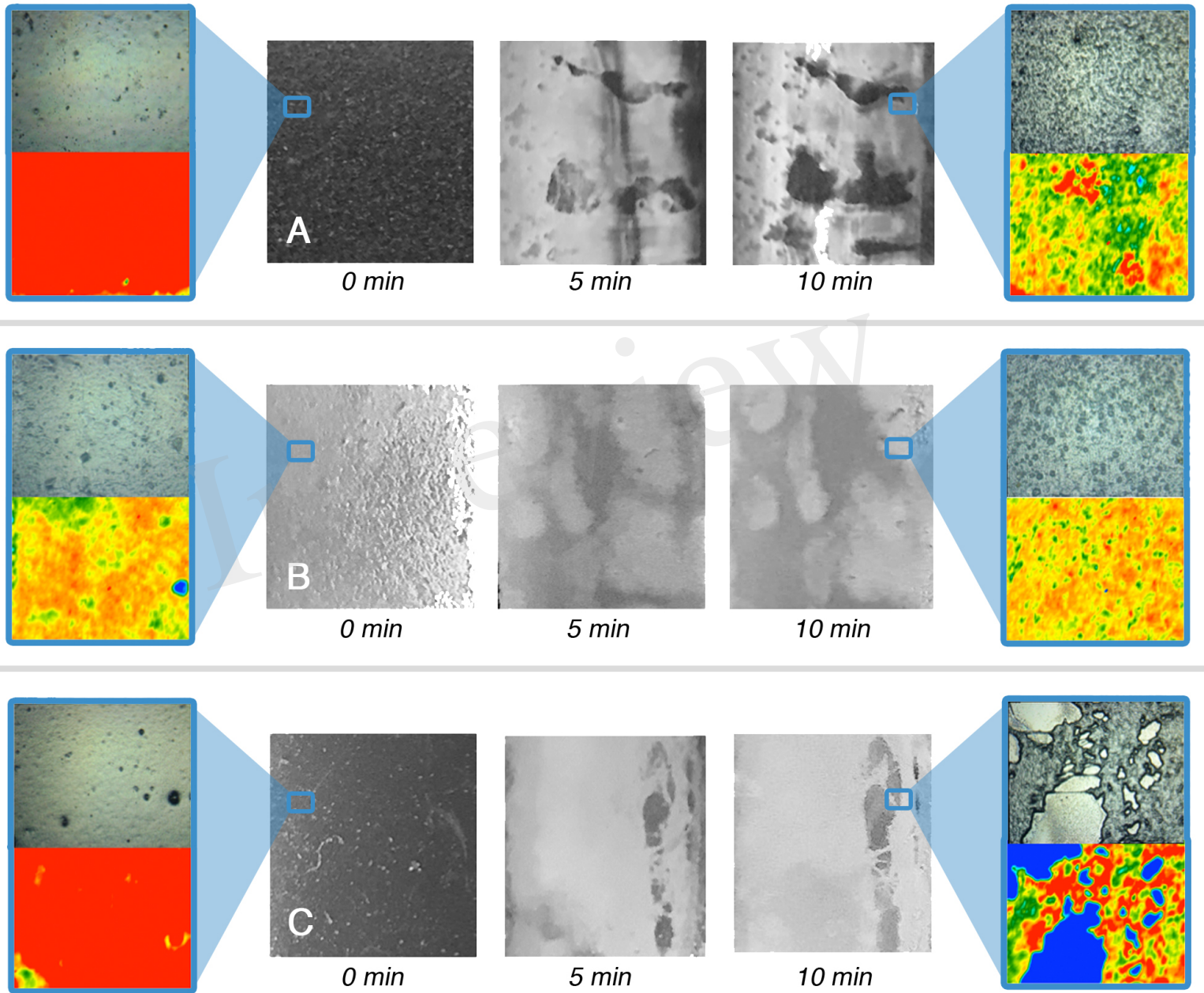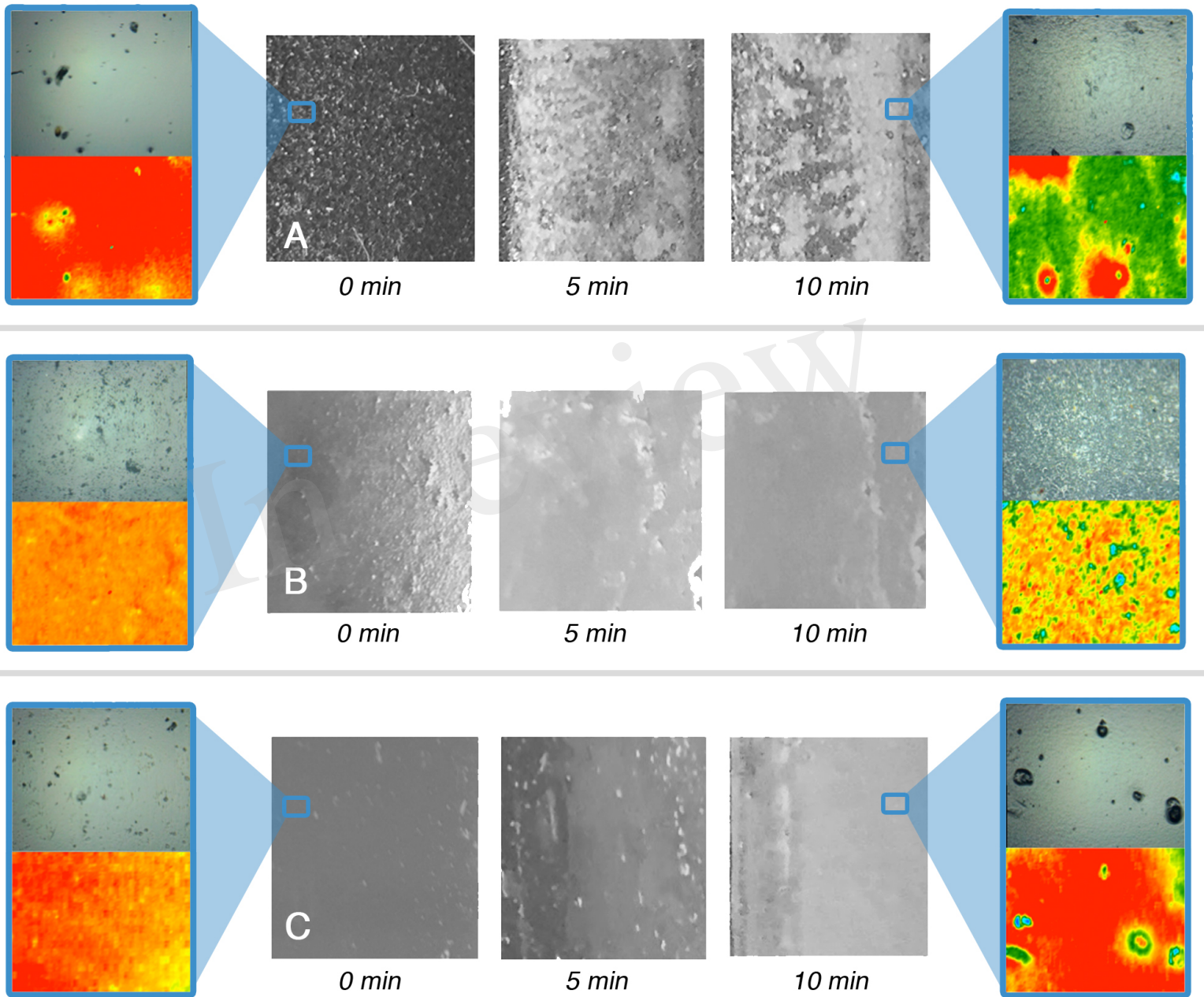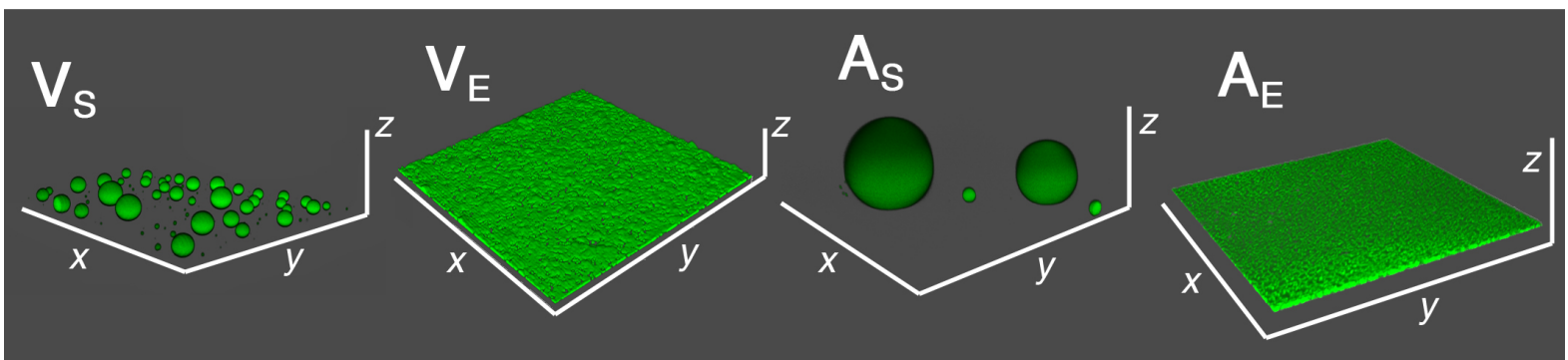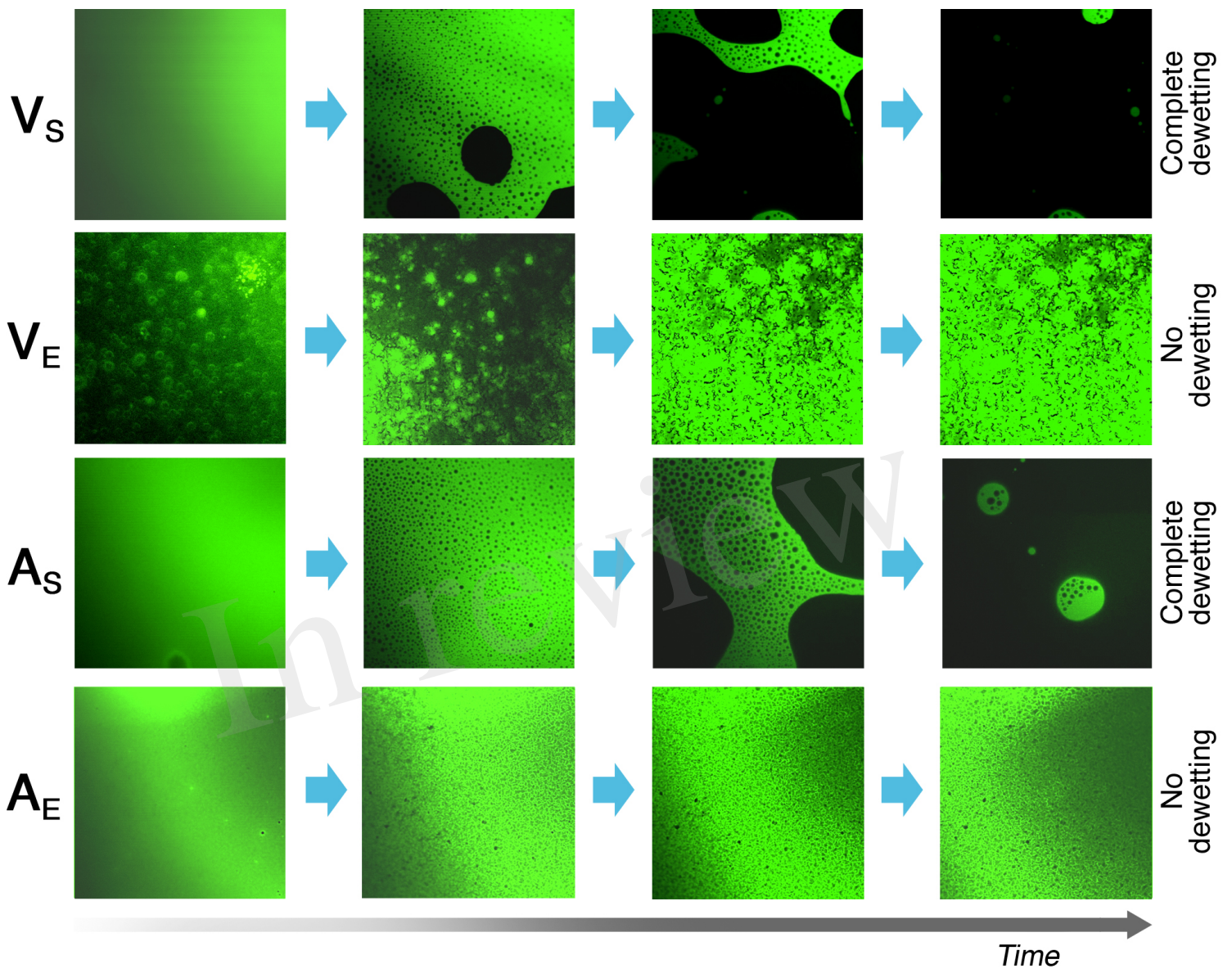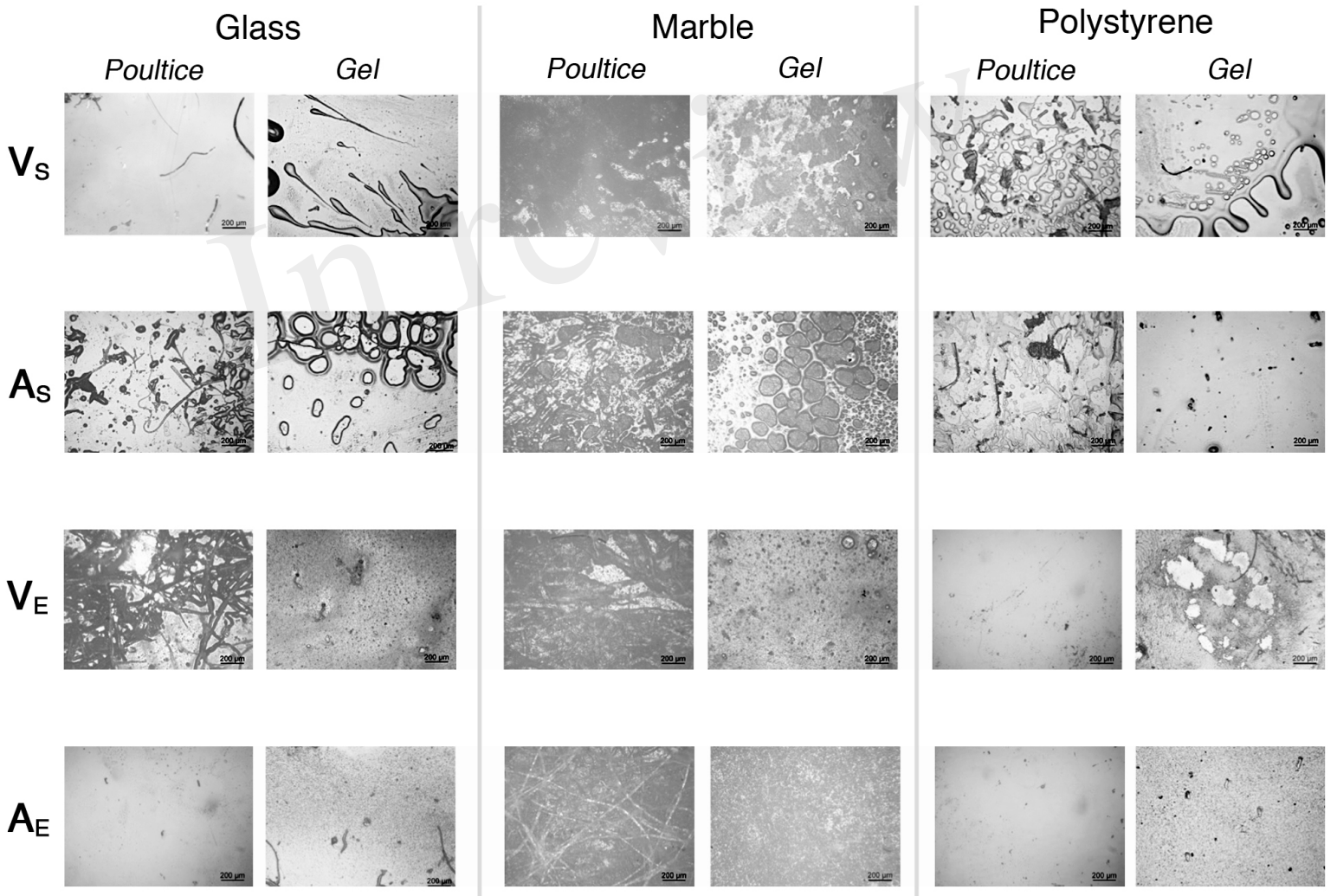
772

Figure 1.JPEG
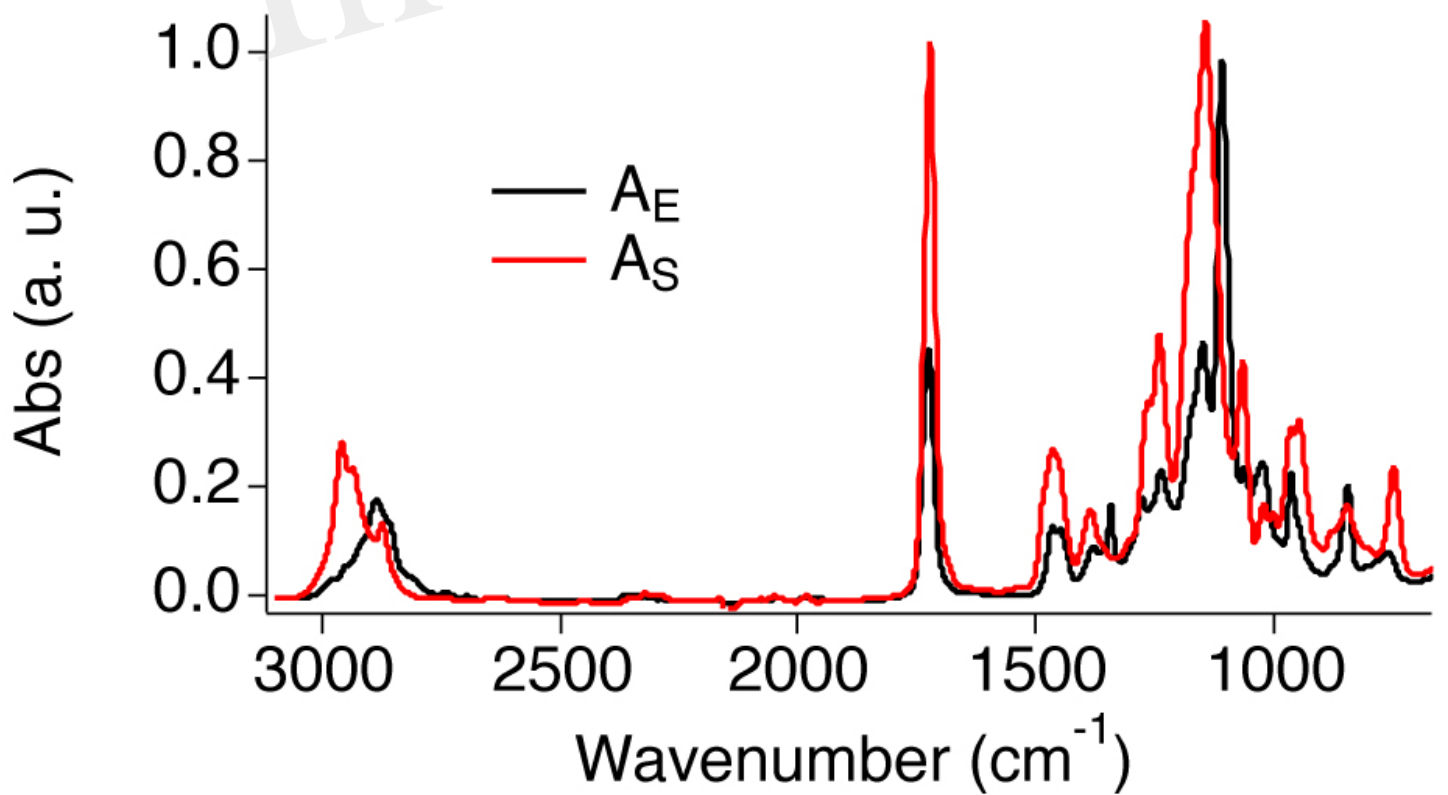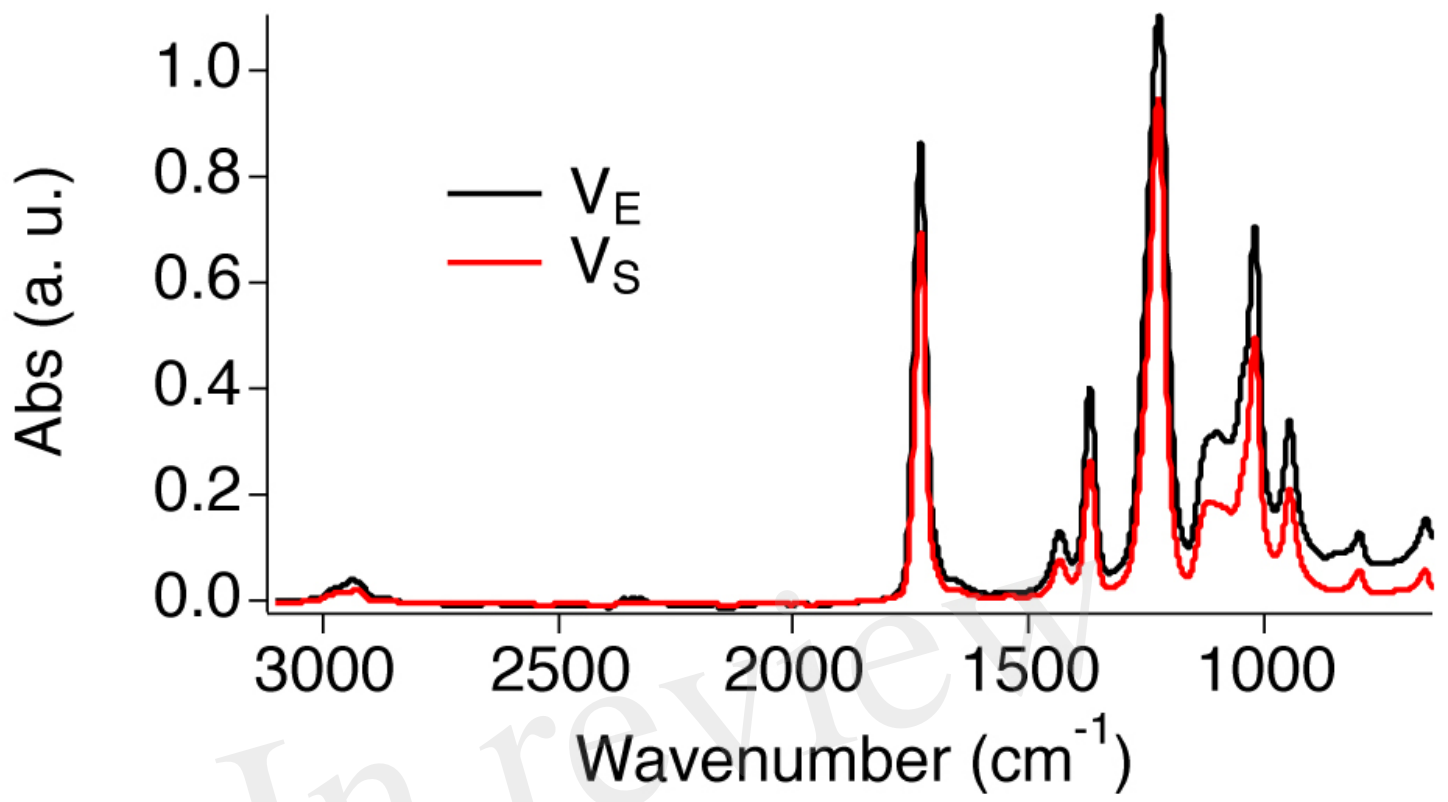
Figure 2.JPEG
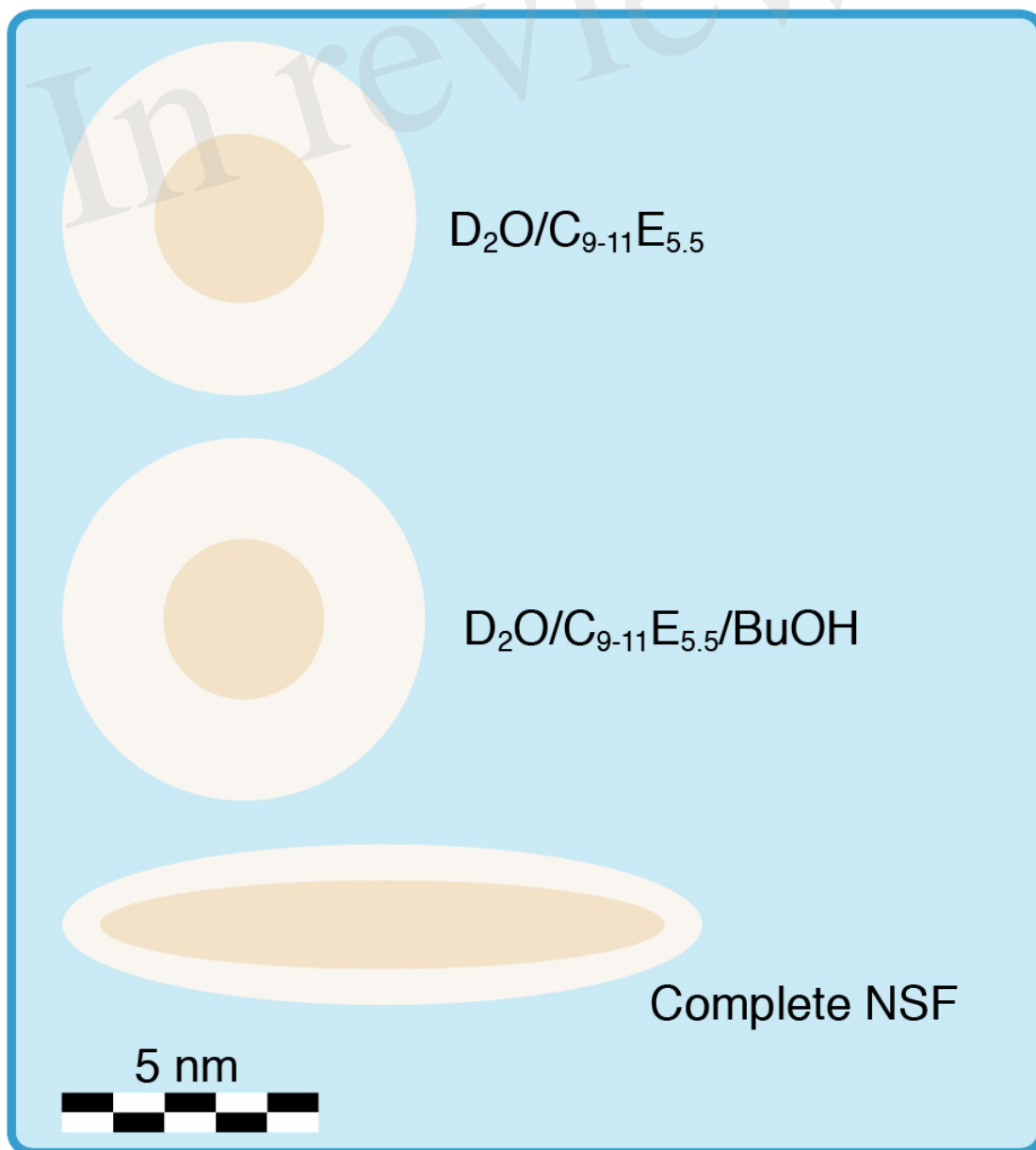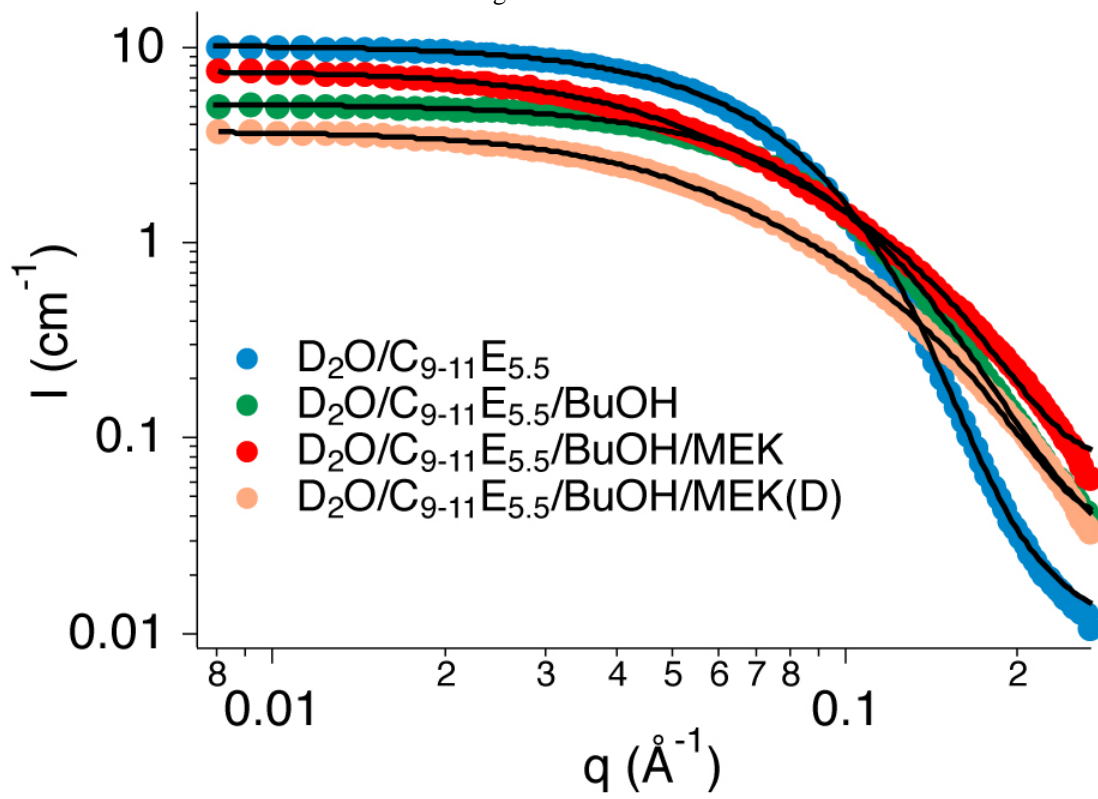
Figure 3.JPEG
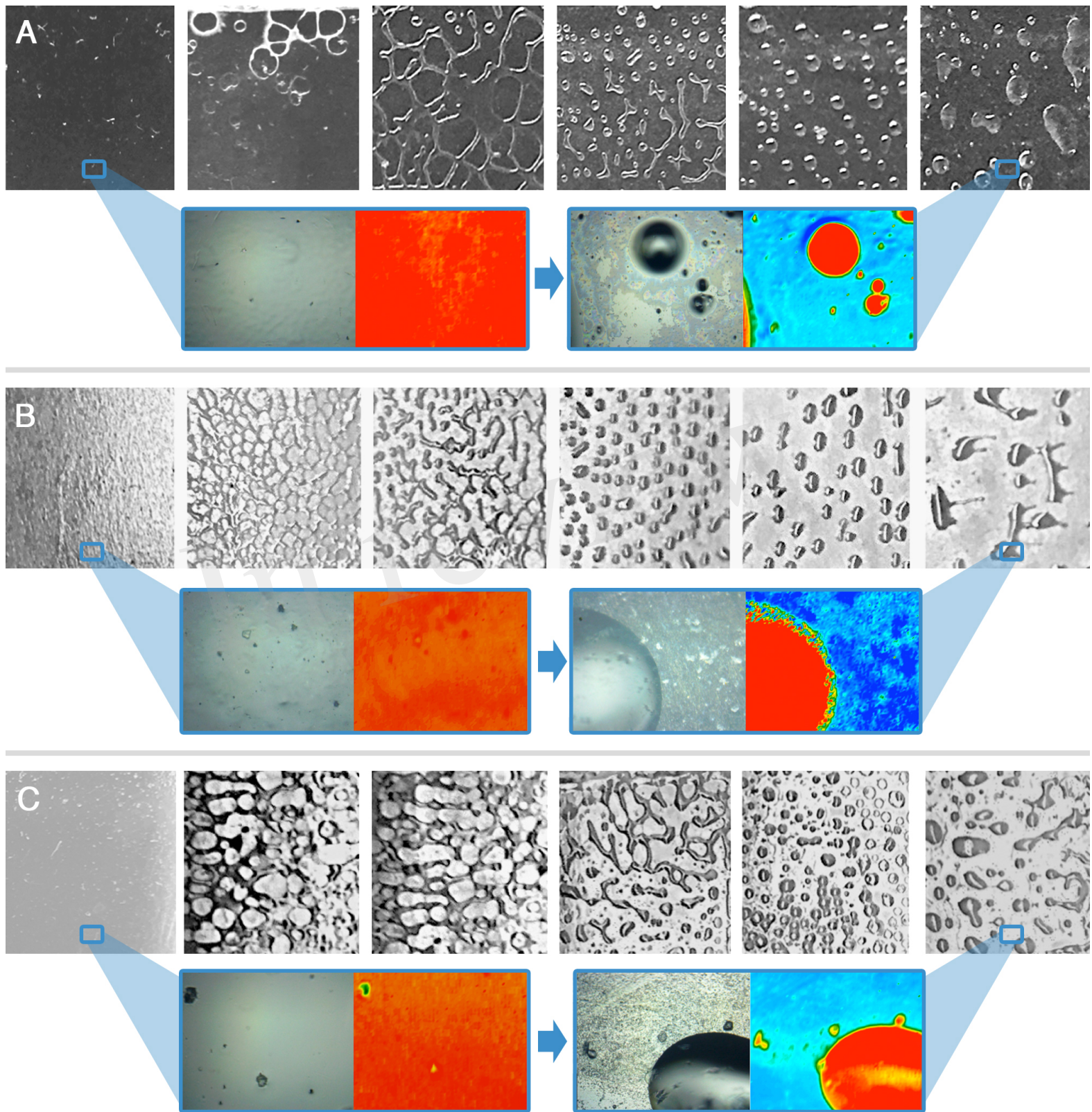
Figure 4.JPEG

Figure 5.JPEG

A   *0 min*   *5 min*   *10 min*

B   *0 min*   *5 min*   *10 min*

C   *0 min*   *5 min*   *10 min*

Figure 6.JPEG

A

0 min *5 min* *10 min*

B

0 min *5 min* *10 min*

C

0 min *5 min* *10 min*

Figure 7.JPEG

V_S — Complete dewetting
V_E — No dewetting
A_S — Complete dewetting
A_E — No dewetting

Time

V_S V_E A_S A_E

Figure 8.JPEG

Figure 9.JPEG